

Exploring High Thermal Conductivity Polymers via Interpretable Machine Learning with Physical Descriptors

Xiang Huang^{1,†}, Shengluo Ma^{1,†}, C. Y. Zhao¹, Hong Wang², and Shenghong Ju^{1,2,*}

¹ China-UK Low Carbon College, Shanghai Jiao Tong University, Shanghai, China

² Materials Genome Initiative Center, School of Material Science and Engineering, Shanghai Jiao Tong University, Shanghai, China

†Equal contribution

ABSTRACT

The efficient and economical exploitation of polymers with high thermal conductivity is essential to solve the issue of heat dissipation in organic devices. Currently, the experimental preparation of functional thermal conductivity polymers remains a trial and error process due to the multi-degrees of freedom during the synthesis and characterization process. Polymer informatics, which efficiently combines data science, machine learning, and polymer experiment/simulation, leading to the efficient design of polymer materials with desired properties. However, available polymer thermal conductivity databases are rare, and establishing appropriate polymer representation is still challenging. In this work, we have proposed a high-throughput screening framework for polymer chains with high thermal conductivity via interpretable machine learning and physical-feature engineering. The polymer thermal conductivity datasets for training were first collected by molecular dynamics simulation. Inspired by the drug-like small molecule representation and molecular force field, 320 polymer monomer descriptors were calculated and the 20 optimized descriptors with physical meaning were extracted by hierarchical down-selection. All the machine learning models achieve a prediction accuracy R^2 greater than 0.80, which is superior to that of represented by traditional graph descriptors. Further, the cross-sectional area and dihedral stiffness descriptors were identified for positive/negative contribution to thermal conductivity, and 107 promising polymer structures with thermal conductivity greater than 20.00 W/mK were obtained. Mathematical formulas for predicting the polymer thermal conductivity were also constructed by using symbolic regression. The high thermal conductivity polymer structures are mostly π -conjugated, whose overlapping p-orbitals enable easily to maintain strong chain stiffness and large group velocities. The proposed data-driven framework should facilitate the theoretical and experimental design of polymers with desirable properties.

* Corresponding author: shenghong.ju@sjtu.edu.cn.

1. INTRODUCTION

Polymers are extensively used in industry and daily life, owing to various advantages of chemical inertness, mechanical flexibility and light weight ¹. As the organic electronics are becoming smaller while the power density keeps increasing, the thermal management and heat dissipation capability have attracted significant attention ². However, conventional polymers are thermal insulators with reported thermal conductivity in the range from 0.1 to 0.5 W/mK, preventing the development of organic electronics ³. Polymers with high thermal conductivity are urgently demanded in organic energy storage and electronic devices to accommodate revolutionary innovations in organic electronics and optoelectronics ⁴. The polymer morphology and topology were found to be closely related to thermal conductivity ⁵. Increasing the crystallite orientation and crystallinity can significantly reduce the phonon scattering and enhance the thermal conductivity along the chain directions, which has been demonstrated by both experiments ⁶⁻⁸ and theoretical simulations ⁹⁻¹². A recent study has fabricated polyethylene (PE) films by disentanglement and alignment of amorphous chains with a metal-like thermal conductivity of 62 W/mK, over two orders of magnitude greater than that of classical amorphous polymers ⁶. Moreover, molecular dynamics simulations have suggested that individual crystalline PE chains have a very high or even divergent thermal conductivity ¹¹. These findings provide opportunities for solving the heat dissipation problem of polymer devices.

Despite the fact that chain alignment, crystallinity, polymer fibers or even single-chain polymer structures exhibit great influence on the thermal characteristic ¹³⁻¹⁵, the polymer library is quite large, with as many as 10^8 monomeric organic molecules known to exist in chemical space ¹⁶. Current research on the thermal conductivity of polymers is still an Edisonian process, guided by intuition or experience in a trial-and-error approach that is time-consuming and expensive ¹⁷. Moreover, most of the studies are conducted on simple structures such as PE ^{4,6,11}, which makes it difficult to grasp the general rule of the factors affecting the thermal conductivity of polymers and to discover polymer molecular structures with high thermal conductivity in huge chemical space.

The field of polymer informatics ¹⁸, associated with the development of artificial intelligence and machine learning (ML) methods, attempts to utilize the data-driven centric method for physical property regulation or device development of organic materials to resolve the conflict between structural freedom and efficiency/cost in the traditional trial-and-error approach. The research on polymer informatics has attracted extensive attention and succeeded in recent years ¹⁹⁻²¹, involving the prediction of organic optical ²²⁻²⁴, electrical ²⁵⁻²⁷ and thermal properties ²⁸⁻³². Particularly, several efforts emerged in the search

or design of structures with high TC as related to crystalline polymers³⁰, amorphous polymers^{31,32} and copolymers³³. Most of these studies have employed graph descriptors³¹ or polymer chemistry fragment statistics^{30,32,33} to describe monomer structures in informatics algorithms, also called fingerprints or representations. The graph descriptors generated rely on molecular/monomer graph information, formulated by knowledge domain feature engineering³⁴ or by attempting to form general descriptors³⁵. Moreover, descriptors such as molecular access systems (MACCS)³⁶ are obtained through statistics of different chemical fragments, and are closely related to molecular graphs. Subsequently, they are collectively referred to as graph descriptors. The fingerprint is required for the unique, complete, minimal representation of each candidate, and the successful fingerprint is a challenging task³⁷. Besides, polymers are composed of many repeating units, which are more complex than organic small molecules and require accurate capture of information on monomer connection sites²⁶. The graph descriptions have long been applied and validated in the development of drug-like small molecules³⁸, and the availability of open-source toolkits such as RDKit³⁹ and Mol2vec³⁴ has facilitated their accessibility, which is also one reason that graph descriptions are popular in polymer informatics. However, the graph descriptor is in the form of a string of numeric vectors. The completeness of the molecular structure determines the coupling association between the digits. Hence, the relationship between molecular monomers and material properties is difficult to grasp.

Exploring the ensemble of physically independent descriptors for the representation of molecular structures is important in qualitative structure-property relationship (QSPR) modeling and enables more intuitive guidelines for molecular structure evaluation⁴⁰. Feature engineering for the collection and reduction of physical descriptors are critical steps in determining effective capabilities in polymer informatics. The development of automatic, universal and efficient tools for the calculation of descriptors of organic molecules is of interest to researchers, which translates the chemical information encoded in the symbolic representation of molecules into useful numbers or some standardized experimental results⁴¹. Several open-source and commercial software⁴¹⁻⁴³ are available to calculate various types of molecular descriptors such as carbon atomic number, molecular weight and Extended Topochemical Atom (ETA)⁴⁴, which have been successfully applied in organic chemistry synthesis⁴⁵, molecular antibacterial activity prediction⁴⁶ and so on. In addition, the parameter conditions in experiments or simulations affect the molecular properties. For instance, the force-field-inspired descriptors such as types of bond, angle and dihedral have been validated for the prediction of the specific heat of polymers, even if the datasets are from experiments²⁹. The number reduction of polymer

features is another concern, as some descriptors may have little relevance to the target property, and a low-dimensional descriptor space is much easier to build up for the ML model ⁴⁷. Feature extraction and selection are the dominant approaches to reduce the dimensionality of features. Feature extraction creates subsets from the original data space, such as principal component analysis (PCA), where the specific meaning of the new features obtained is difficult to understand ⁴⁸. Feature selection retains the physical meaning of individual descriptors, while filters based on correlation evaluation have dependencies on mathematical models, like the Pearson and Spearman coefficients that consider the linear and monotonic relationships of the data, respectively ⁴⁹. Further, the filter methods do not involve ML models, which may lead to the inapplicability of the gained features. The wrapper-based feature selection techniques combine ML models to eliminate redundant features, including recursive feature elimination (RFE), sequential feature selection (SFS) and exhaustive feature selection (EFS) ⁵⁰. Testing different subsets of descriptors for informatics algorithms is the crucial feature of the wrapper approaches, and the key is the strategy of combining different descriptors. Typical RFE seeks to improve model performance by continuously reducing the low impact features from the remaining features in iteratively constructed ML models, which refer to the ranking of feature weights assigned by models such as random forests ⁴⁸. Thus, the RFE relies on the feature weight evaluation mechanism of the ML models.

Herein, focusing on the challenges of polymer monomer representation and feature selection, we proposed an ML interpretable framework integrated with high-throughput MD simulations for the discovery of polymer structures with high TC, as illustrated in Fig. 1. It consists of four components: 1) polymer library construction, 2) MD simulation for the TC of polymers; 3) monomer feature representation and hierarchical down-selection; 4) ML models construction for TC prediction. The training data was collected from the literatures ^{51,52}, and candidates from the databases of PolyInfo ⁵³ and PIIM ⁵⁴ were applied for the virtual screening of high TC structures. All polymer monomers were identified by the SMILES (simplified molecular input line entry system) strings and formed one-dimensional polymer chains by replication. The TC of training datasets was calculated by MD simulations with the second generation of the general AMBER force field – GAFF2 ⁵⁵. Inspired by drug-like molecular representation and molecular force fields, we obtained 320 physical descriptors by mordred software ⁴¹ calculation and force field parameter file extraction, and retained 20 optimized descriptors by hierarchical down-selection. We then trained random forest (RF), extreme gradient boosting (XGBoost) tree-based models, and multilayer perceptron (MLP) neural network model

separately to establish the relationship between the optimized descriptors and the TC of these benchmark polymer datasets. Further, we analyzed the feature importance of each optimized descriptor and extracted the chemical heuristic for high TC polymers design through SHAP analysis⁵⁶. Using the trained ML models, 107 promising polymers with TC greater than 20.00 W/mK were identified, which are served for symbolic regression to derive mathematical formulas for expressing the TC of promising polymers. Last, we discussed the TC mechanisms of eight typical polymers. Overall, the proposed approach is beneficial for theoretical or experimental investigations of high TC polymers.

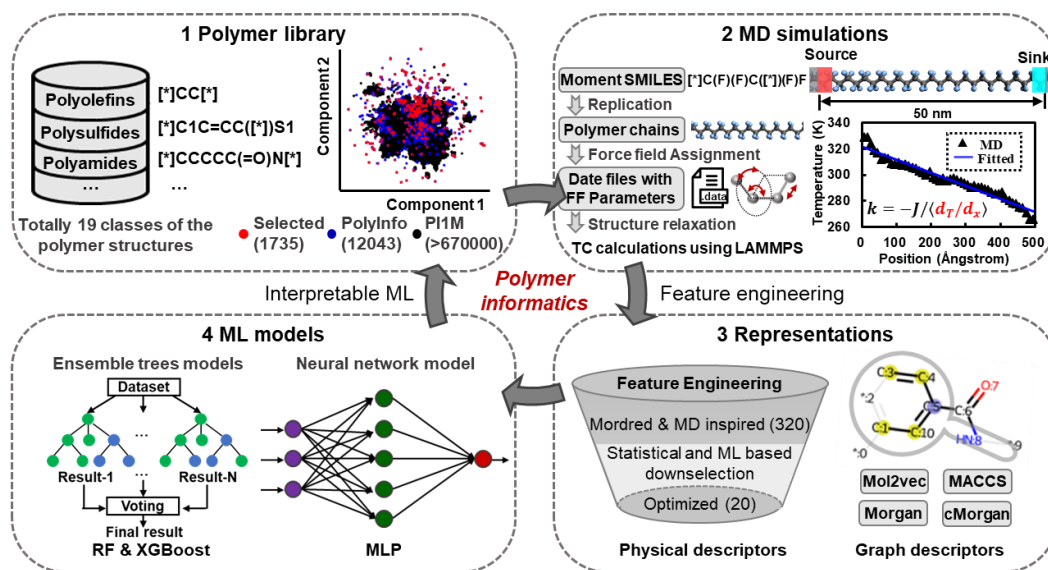


Fig. 1. Schematics of high-throughput screening of polymers with high TC via interpretable machine learning.

2. RESULTS AND DISCUSSION

2.1 Distribution of polymer datasets in chemical space

Polymer data from literatures^{51,52} were utilized as the benchmark database for training machine learning models, as well as PolyInfo⁵³ and PI1M⁵⁴ databases were used for the virtual screening of polymer structures with high TC. The polymers are classified into 19 classes such as polyolefins, polyethers and polyamides according to different elements and chemical functional groups⁵⁷. To validate the distribution of the selected 1735 benchmark data over the other two datasets, their chemical structures were visualized in 2D space by the uniform manifold approximation and projection (UMAP)⁵⁸, where the chemical structure of each monomer was transformed into the Morgan fingerprint³⁵ of a 1024 vector with a radius of 2 atoms. It is observed that the polymer structures in the selected benchmark dataset (Fig. 2a) are well covered by the chemical space distribution of those in the PolyInfo (Fig. 2b)

and PI1M (Fig. 2c) databases. Note that the PI1M dataset was generated by a generative model of a recurrent neural network trained with data from PolyInfo, which fills the sparse region of the chemical space of the PolyInfo dataset, but the distribution is consistent⁵⁴. Thus, the ML models trained with the selected data are well able to learn the chemical features of all candidates and can be effectively adopted for the virtual screening of polymer structures with high TC.

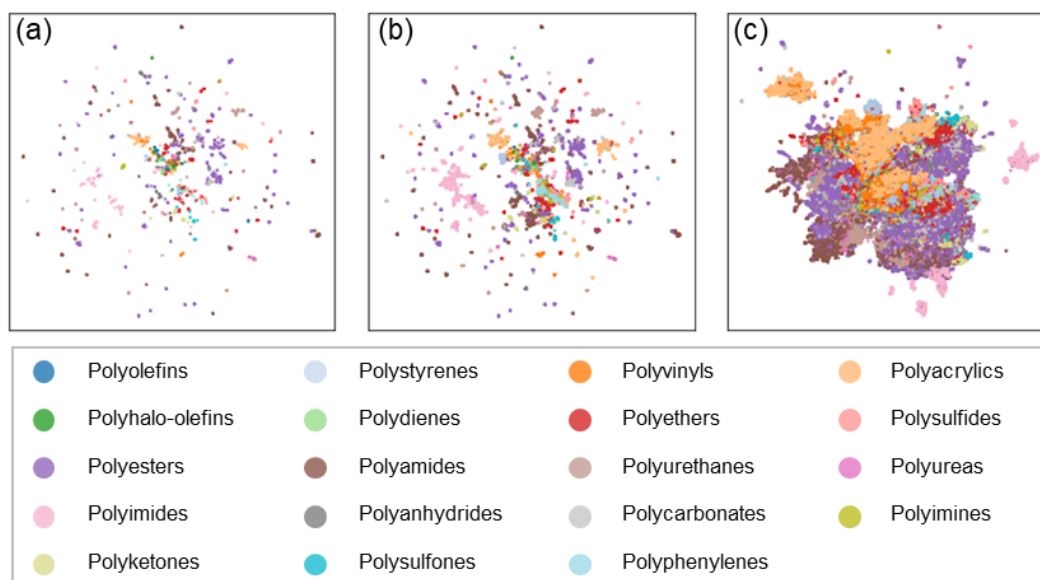


Fig. 2. Visualization of polymer data distribution in a 2D space by UMAP. (a), (b) and (c) are corresponding to the selected, PolyInfo and PI1M datasets, respectively.

2.2 Polymer descriptors hierarchical down-selection and ML Models Training

Polymer descriptors are hierarchically down-selected in three stages: removing features with low variance, primary filtering referred to different correlation coefficients, and final selection assisted with the ML model (shown in Supplementary Section S1). The collected initial monomer physical descriptors are composed of 286 Mordred-based and 34 MD-inspired descriptors. The descriptors of MD-inspired and Mordred-based descriptors are listed in Supplementary Section S2. The removal of low variance descriptors is intended to eliminate descriptors with variance less than a specific threshold, whose contribution to the target property of all polymer data (TC in this work) is considered to be nearly consistent. After the variance threshold was set to 0.01, the 264 descriptors were reserved for the next stage. We established the weight assignment mechanism (WAM) based on the different correlation coefficients for further primary filtering of the descriptors, due to the various attentions of their mathematical models. The Pearson, Spearman and Distance coefficients are used to evaluate linear, monotonic and non-linear relationships between data respectively, while the maximum information coefficient (MIC) reflects the association of two variables through information entropy, whether linear

or nonlinear. The reliability of MIC depends on the data sample size and the value is reliable only with large datasets. The four metric coefficients of Pearson, Spearman, Distance and MIC were incorporated and each was assigned a weighting factor of 0.25, and the thresholds were set to 0.05, 0.05, 0.153 and 0.132, respectively. The 53 descriptors with a cumulative weight value of 1 were retained through VAM. Random sequential feature selection (RFSF) combined with the RF model was then developed for optimized descriptors determination. Considering all possible combinations of descriptors for ML model training is time-consuming and expensive, so traditional SFS usually leads to sub-optimal solutions, where the recommended ensemble of optimized descriptors is not unique, and is influenced by the input order of the descriptors⁵⁹. Here, we disrupted the order of the input descriptors, combined them with 100 RF model training cycles, and acquired the final optimized descriptors based on a statistical approach. The threshold was set to 0.34, that is to maintain descriptors that occur more than 34 times in 100 RF model training runs. The results of the optimized descriptors based on VAM and RSFS are shown in Fig. 3a and their detailed descriptions are listed in Supplementary Section S3. Moreover, Fig. 3e exhibits the Pearson correlation matrices of the correlations among optimized descriptors (Other metrics see in Fig. S1). It is found that most descriptors are positive correlated with each other and negative correlated with TC. Only three descriptors are positive for TC, two of which are MD-inspired descriptors. For example, the descriptor MW_ratio reflects the ratio of the molecular weight of the mainchain to the molecular weight of the monomer, with values between 0 and 1. The MW_ratio of 1 indicates that the polymer is without side chains, which reduces the loss of heat flux along the chain and makes it possible to get large TC.

Figure 3b shows the results of the RF model trained with the optimized descriptors, with training and test R^2 of 0.87 and 0.84 respectively. To verify the extensibility of the optimized descriptors, XGBoost and MLP models were deployed for training (see Fig. S2). The accuracy of the training and test sets for XGBoost is 0.95 and 0.87, and that for MLP are 0.81 and 0.88 respectively, which is comparable or even better than the RF model. Therefore, these three models are utilized in the subsequent discussion.

The prediction accuracy of ML models at different down-selection stages illustrated in Figure 3c (training and test data set prediction in Fig. S3). The extra PCA more than 95% variance was performed to compare with RFSF technology. According to the relationship between the number of principal components and the cumulative variance in Fig. S4, at least 19 components are required to exceed 95% variance. This is close to the number of sets of optimized descriptors. As seen in Fig. 3c, the tree-based

models of the RF and XGBoost maintain relatively high accuracy even with large descriptor dimensions because of their strong ability to prevent overfitting of the data. Moreover, the feature down-selection process is usually accompanied by the loss of information, which results in the decrease of model accuracy. However, the feature down-selection process also reduces the redundancy between data which suppresses the overfitting and improves the accuracy of the MLP model. Overall, the accuracy of all three models trained with the optimized descriptors from RFSF is higher than that of the models trained with the PCA-derived descriptors, which demonstrates the effectiveness of our approach.

The ML models with different graph descriptors were applied for comparison in Fig. 3d (training and test data set prediction in Fig. S5). The Mol2vec³⁴ is an unsupervised ML approach to learn vector representations of molecular substructures, which requires a benchmark dataset for molecular structure training. Here, the pre-trained polymer embedding model was from elsewhere⁵⁴, which was created using the PolyInfo and PIIM datasets. The MACCS³⁶ descriptor is the structural key-based descriptor with 166-bit keyset. The Morgan and Morgan count (cMorgan)³⁵ descriptors are the extended connectivity fingerprints that capture molecular features relevant to molecular activity. The results in Fig. 3d reflect the superiority of ML models trained with the optimized descriptor, no matter the models of RF, XGBoost and MLP. The down-selection processes of physical descriptors examine individual/combined descriptors in relation to TC, while the graph descriptors aim to represent molecular/monomeric information as completely as possible. Whilst the elements or groups in the molecular graph have been indicated to correlate with the TC of polymer chains³⁰, it is more intuitive and effective to predict the TC of polymer chains using the associated physical descriptors. But not absolute, which is also related to the parameters such as chain stiffness⁶⁰.

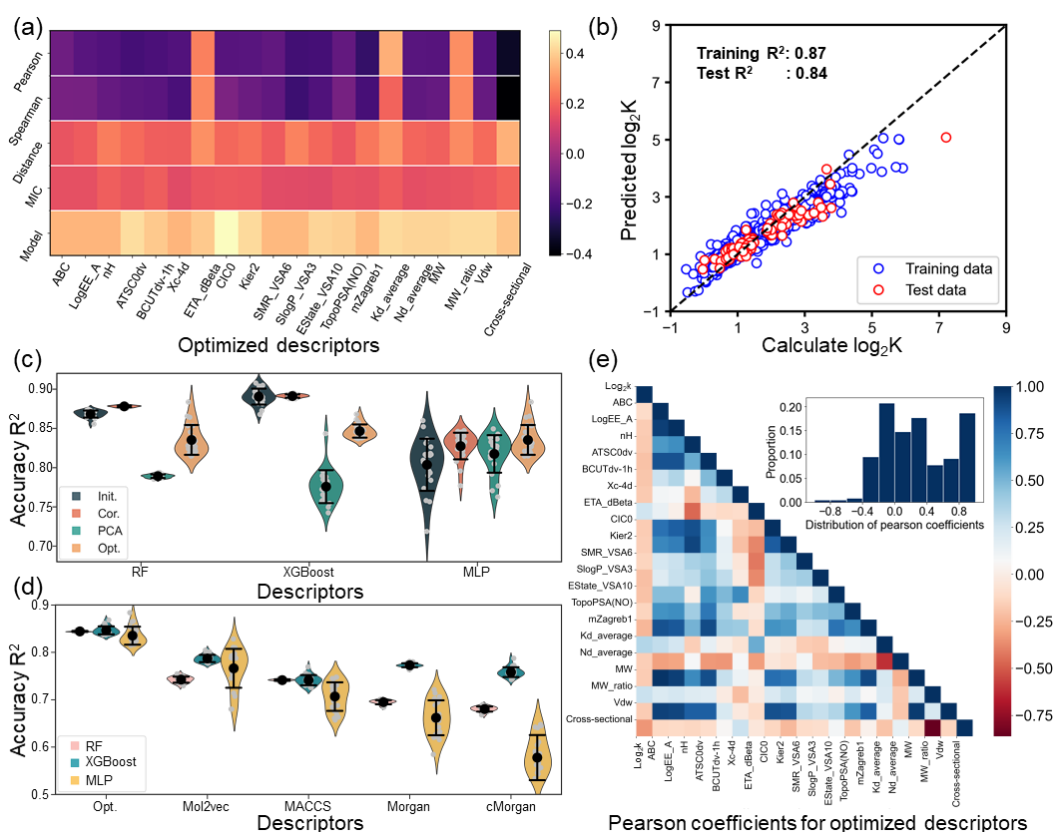


Fig. 3. Polymer descriptors down-selection and ML models training. (a) Optimized descriptors acquired by down-selection with four coefficients - Pearson, Spearman, Distance, and MIC coefficients - and RF model. (b) Accuracy of RF model based on optimized descriptors, where training R^2 is 0.875 and test R^2 is 0.844. (c) Accuracy of ML models at different down-selection processes, including initial (Init.), mathematical correlation (Cor.) coefficients screening and RF model optimization (Opt.) stages. And, an additional PCA approach was applied to compare. (d) Accuracy of ML models with different polymer representation approaches. The violin plot represents the distribution of values, individual subsamples are shown in gray, and the mean and standard of R^2 in black. (e) Pearson correlation matrices showing correlations among optimized descriptors and TC. The inset is the statistics of the Pearson coefficients distribution.

2.3 Physical insights from interpretable ML model

Figure 4 summarizes the effect of the features using SHAP, for the RF model trained on optimized descriptors. The SHAP approach attempts to address the unexplainable black-box challenge of ML algorithms by calculating the marginal contribution of features to the model output⁵⁶. Hence, the features of each polymer structure in training data sets are assigned the SHAP values separately. As shown in Fig. 4a, the importance ranking of the optimized descriptors was referenced to the average SHAP value. Among the top 8 optimized descriptors, the number of MD-inspired and Mordred-based descriptors is equal, which reflects the fact that the construction of the RF model is a joint contribution of these two types of descriptors. The distribution of SHAP values for each descriptor is displayed in Fig.4b, and the depth of shade of datapoints in the beeswarm plot represents the magnitude of TC of

polymer structures in the training set. The distribution of SHAP values for the top-ranked features is relatively wide, and is monotonic about the feature values overall (Fig. S6).

Here, we highlight the two MD-inspired descriptors of cross-sectional and Kd_average. The most important descriptor of cross-sectional indicates the effective cross-sectional area of polymer chain, which is intuitive in relation to the TC. From the Fig. 4c, the SHAP value for cross-sectional decreases monotonically with the descriptor. According to the Fourier's law, the heat flow rate along 1-D polymer chain can be expressed as $Q/d_t = -kA d_T/d_x$, where Q is the heat flow, d_t is the time interval, k is the thermal conductivity, A is the cross-sectional area, and d_T and d_x are the temperature difference and distance between the hot and cold ends, respectively⁶¹. Therefore, the TC is negatively related to the cross-sectional area, and polymers with high TC usually have a small cross-sectional area (Fig.S7a). Moreover, the polymer chain structure is absent of disorder compared to the amorphous structure, maintaining the symmetry of the crystal and reducing phonon scattering. However, the polymer chains may rotate and become disordered due to temperature and other effects, resulting in a rapid decrease in TC⁶². The closely correlation between dihedral angle energy constant and polymer chain stiffness has been demonstrated, and the dihedral angle force constant Kd has been artificially increased in MD simulations to maintain PE chain stiffness and increase thermal conductivity^{62,63}. The Kd_average is the average of all types of dihedral force constants from GAFF2 force field for polymer chain, which is roughly proportional to the corresponding SHAP value in Fig. 4d. Especially for polymer structures with great kd_average (>4 kcal/mol) usually have large SHAP values and TC (Fig S7 b). Notably, the TC of polymer chains is influenced by multiple parameters and it is difficult to have the individual descriptor to determine its value. One example is that crystalline polynorbornene has been proved to be weakly sensitive with the chain stiffness, even if increasing the dihedral angular force constant term in MD simulations⁶². This confirms the significance of our proposed ML framework for predicting the TC of polymers.

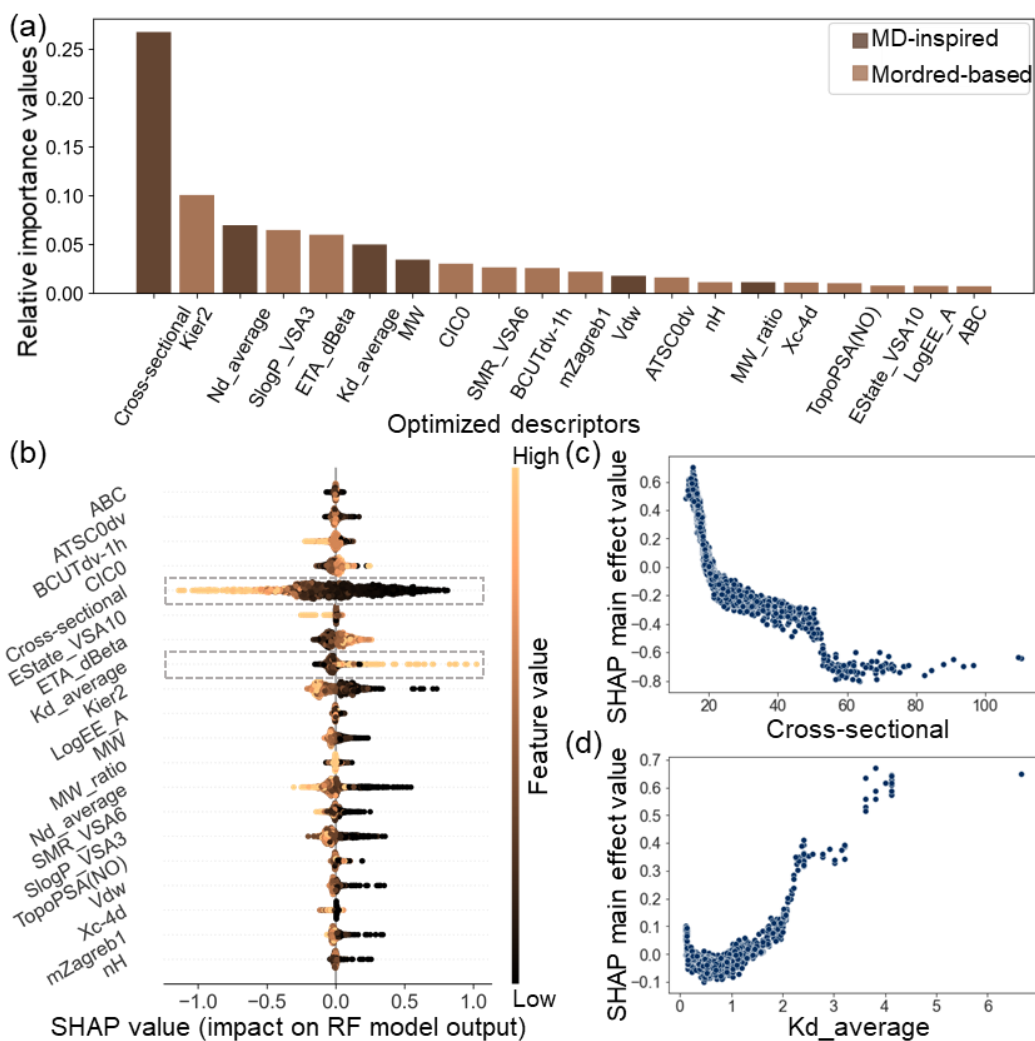


Fig. 4. Analysis of feature importance using SHAP on RF model trained by optimized descriptors. (a) Average SHAP values for 20 optimized descriptors. (b) Represent the SHAP values of each descriptor related to training data set polymers in a beeswarm diagram. (c) and (d) SHAP values for the Cross-section and Kd_average of the training data set polymers as a function of descriptor value. The Cross-section is the effective cross-sectional area of polymer chain, and the Kd_average is the average value of force constants of the dihedral angle from GAFF2 force field.

2.4 Discovery of high TC polymers

The optimized descriptors were validated reliability in combination with different ML models for predicting the TC of polymer chains. Next, we applied these ML models to predict the TC of polymer structures in the PolyInfo and PI1M databases, in order to virtually screen promising polymers with high TC. The predicted polymer TC versus cross-sectional area from the ensemble of optimized descriptors combined with RF, XGBoost and MLP are visualized in Fig. 5a-c, respectively. Where stars indicate polyethylene with \log_2 TC of 3.91, 4.66, and 5.30 predicted by RF, XGBoost, and MLP

respectively, and that calculated by MD simulation is 5.28. The dependence of TC on the cross-sectional area is evident here, as almost all of the predicted high TC polymers have small cross-sectional areas. Moreover, since PI1M has the same chemical distribution space as PolyInfo and fills the sparse area, which covers most of the TC range of PolyInfo and enriches the polymer structures in the high TC region.

Comparing the results from different ML models, the tree-based models of RF and XGBoost predict the TC of polymers in a narrower space than that of the MLP. Though the excellent performance of the tree-based models in preventing overfitting, the extrapolation of the models is usually inadequate and the predictions are still limited to the range of TC of the polymer structures in the training set. In contrast, neural network model of MLP usually has better extrapolation capability, and is superior in finding small data such as high TC polymer structures, despite the relatively low training accuracy R^2 of the model. This finding is similar to previous study of predicting the permeability of gas separation membranes using ML¹⁷. As well, previous work has revealed the length dependence of the thermal conductivity of polymer chains. Within a certain length range, the diverging thermal conductivity k and chain length L can be fitted by $k \sim L^\beta$, where β indicates the relatively dominant phonon transport mechanism¹³. Here, we considered polymer chains with TC greater than 20.00 W/mK with an effective length of 50 nm as the outstanding polymers with high TC. Then, balanced strategy to integrate the three ML models performance were devised to recommend promising polymer structures for calculation of TC by MD simulations. We identified the polymer structures in the PolyInfo dataset with RF, XGBoost and MLP predictions of \log_2TC up to 3.51, 3.50 and 4.33, and only the polymer structures with no less than 2 occurrences were picked for MD simulations. As a result, 24 polymer structures with high TC were discovered and verified. Similarly, we implemented this method to identify 84 high TC polymer structures in the PI1M database. After de-duplication, totally 107 high TC polymer structures were found in this work, and the Synthetic accessibility (SA) scores were calculated as shown in Fig. 5d. The specific polymer structures can be seen in Supplementary Section S8. From Figure S8, we can see that most of the high TC polymers are simple linear or contain aromatic rings in the mainchain, which have small repeating unit lengths and no side chains. The SA score was initially utilized to estimate the synthetic accessibility of drug-like molecules based on molecular complexity and fragment contributions⁶⁴, and was subsequently adopted for polymers^{31,32}. The SA score values ranged from 1 to 10, and synthesis is more difficult as the value increases. To take into account the effect of monomer linkages, polymer molecules with a polymerization degree of 6 were calculated for the SA score. Among

them, 28 polymer structures with SA no more than 3.00, including polyethylene, polytetrafluoroethylene and poly(p-phenylene), and etc. Although it is currently difficult to fabricate each of these structures, we believe that more polymers like PE chain will be prepared for exploring the limits TC of polymers by combining advanced processes such as micromechanical stretching, electrostatic spinning and nanotemplate preparation in the near future ^{4,6,11}.

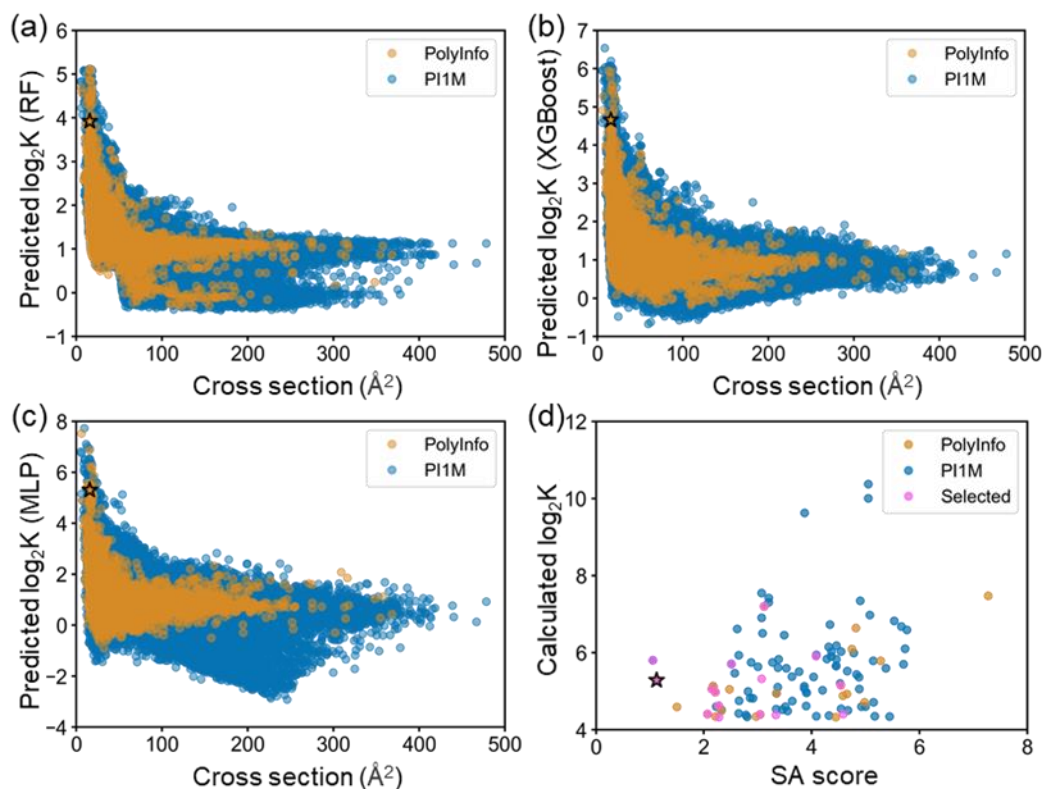


Fig. 5. Prediction of high TC polymers in PolyInfo and PI1M databases using constructed ML models. (a), (b) and (c) based on RF, XGBoost and MLP models, respectively. (d) Synthetic accessibility (SA) score versus calculated $\log_2 K$ of screened high TC polymers ($TC > 20.00$ W/mK). The star indicates PE, and the TC in this work is 38.98 W/mK.

2.5 Symbolic regression for prediction of promising polymers

Since the TC of polymer chains is influenced by complex multi-parameters, it is difficult to predict trends in TC values for different polymers from any single descriptor. Symbolic regression (SR) attempts to accelerate the discovery of materials with superior properties by relating available descriptors through mathematical formulas to construct new combinatorial features ⁶⁵. SR does not require massive datasets, as long as a high consistency and accuracy ^{66,67}. The 107 promising polymer structures ($TC > 20.00$ W/mK) with optimized descriptors were utilized for SR, where the ratio of training to test set was 3:1. The mathematical formula were acquired and selected using an efficient stepwise strategy with SR based on genetic programming (GPSR) as implemented in the gplearn code

⁶⁸. The hyperparameters setup and the detailed formula determination process can be found in Supplementary Section S9. Pearson coefficients are first applied to filter optimized descriptors and create sub-descriptors, and a novel ensemble of 22 descriptors was obtained. The frequency of occurrence of optimized descriptors in 158 mathematical formulas (PC values ≥ 0.85 and complexity ≤ 10) is displayed in Fig. 6a, and first 8 descriptors were finally retained. It is worth emphasizing that the MD-inspired descriptors of cross-sectional area (cross-sectional) and dihedral force constants (Kd_average) appeared in each of the formulas. In Figure 6b, we calculated the Pearson coefficients of the new set of descriptors with the TC, the results suggest these descriptors are closely associated with the TC. Subsequently, we reset the grid search hyperparameters in gplearn and used R^2 as the evaluation metric. Only formulas with high R^2 and low complexity (length of formula) are considered suitable for the prediction the TC of polymer structures ⁶⁹. Thus, 9073 mathematical formulas with complexity within 30 and R^2 over 0.6, which are characterized by complexity and accuracy R^2 via density plot in Fig. 6c. The four points of c, d, e and f at Pareto front were identified by Latin hypercube sampling approach ^{70,71}, and their corresponding formulas are expressed in Table S8. The complexities of the four formulas are in the range of 20 to 30, and the fitting accuracies are all greater than 0.70. Moreover, the training accuracy is mostly positive to complexity. For example, the formula represented by point c with complexity of 20 has a relatively low accuracy R^2 among the four points, but the fitting results are consistent with the MD labeled $\log_2 K$, as demonstrated in Fig. 6d. Meanwhile, all four identified formulas include the descriptors of the Cross-sectional, Kd_average and Nd_average, which verified that the TC of polymer chain is strongly correlated with the parameters such as cross-sectional area and dihedral stiffness. These formulas are meaningful in the initial rapid screening of high TC polymer chain structures.

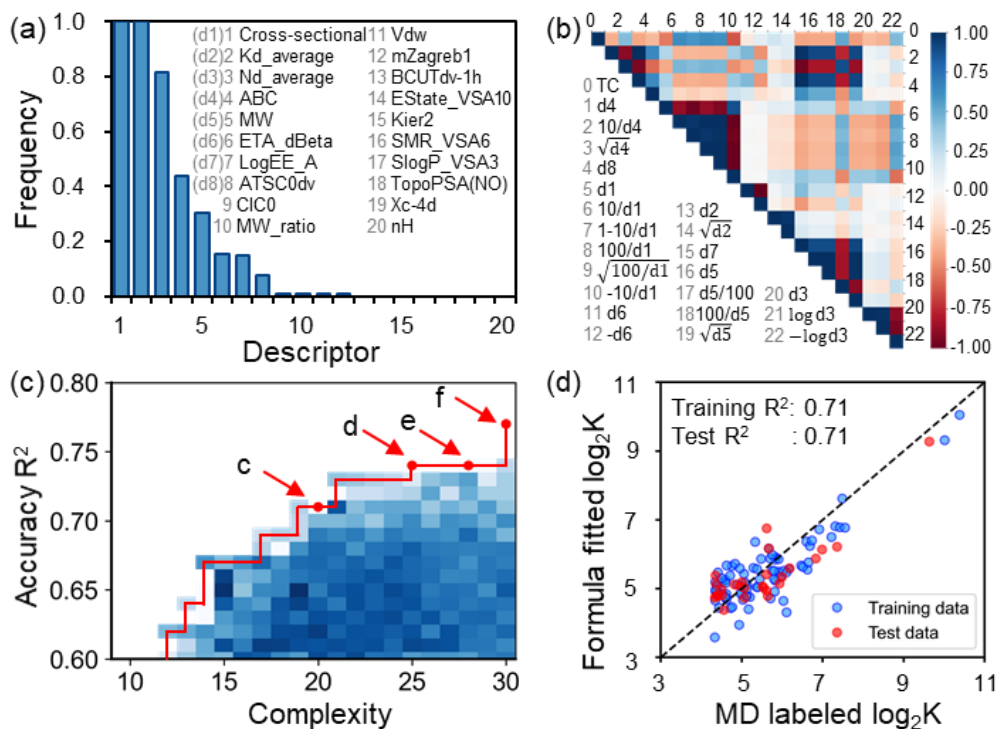


Fig. 6. GPSR for TC prediction of promising polymers. (a) Frequency of occurrence of optimized descriptors in 158 mathematical formulas (PC values ≥ 0.85 and complexity ≤ 10). (b) Pearson correlation matrices showing correlations among 22 descriptors and TC, where the descriptors d1~d8 correspond to descriptors 1 to 8 in Fig. 6a. (c) Pareto front of accuracy R^2 vs. complexity of 9073 mathematical formulas shown via density plot. (d) MD labeled vs. fitting results of the formula (point c) with complexity of 20 and training accuracy R^2 of 0.71.

2.6 Thermal transport mechanism of promising crystal polymers

Taking into account factors such as TC and SA score, eight polymer structures (see in Fig. 7a) were chosen for the analysis of phonon dispersion relations. Currently, polymer structures like $[*]C=C[*]$ and $[*]N=N[*]$ are challenging to be synthesized experimentally, but are contributing to our understanding of polymer thermal conductivity mechanisms. All of these polymer molecules are π -conjugated structures except for the PE and the Polytetrafluoroethylene (PTFE), which are simple linear structures. In π -conjugated polymer molecules, the overlap of p-orbitals has enhanced restraint in inhibiting chain rotation and forming the rigid backbone¹². Figure 7b illustrates the phonon dispersion relations, which were obtained by phonon spectral energy density (Phonon-SED) analysis⁷². The detailed description of the Phonon-SED approach can be found in the Method part. Since the acoustic modes are dominated by the thermal transport of heat carriers in polymer crystals, phonon modes with frequencies below 25 THz are demonstrated. Moreover, the phonon group velocity is approximated as

the average of the slopes of all acoustic branches^{12,60}. In the one-dimensional polymer chain systems, the TC is analyzed as $k = v_g C_v l$, where v_g is the phonon group velocity, C_v is the volumetric heat capacity and l is the phonon mean free path. Due to the limitation of classical MD simulations, the volumetric heat capacity can be expressed as $C_v = 3k_b N/V$, where k_b is Boltzmann constant, N is the number of atoms and V is the volume. Thus, phonon mean free path can be calculated by the ratio of the TC to the multiplication of the phonon group velocity and the volumetric heat capacity. The approximations of the above calculations allow the results to be rough, but it do help us to understand the underlying thermal conductivity mechanisms of these promising polymer structures by comparing the relative trends of the relevant parameters, as listed in Table 1.

The volumetric heat capacity of the eight polymer structures varies from 3.28 to 6.13, which is not critical to the high TC of polymer chains. As for the phonon group velocity, the six π -conjugated polymers have large values (more than 5900 m/s) due to overlapped p-orbital and delocalized electrons. Additionally, the small atomic mass enables a large phonon group velocity. The PTFE has smaller phonon group velocity than that of PE due to the relatively larger mass of fluorine atoms compared to hydrogen atoms. The phonon mean free path provides valuable insights into phonon transport in the polymer chains. Overall, simple linear polymer chains are easily to have long phonon mean free paths, especially for linear π -conjugated polymers of $[*]C=C[*]$ and $[*]N=N[*]$. These structures have large chain stiffness and few atoms except for the backbone, thereby having weak phonon-disorder scattering.

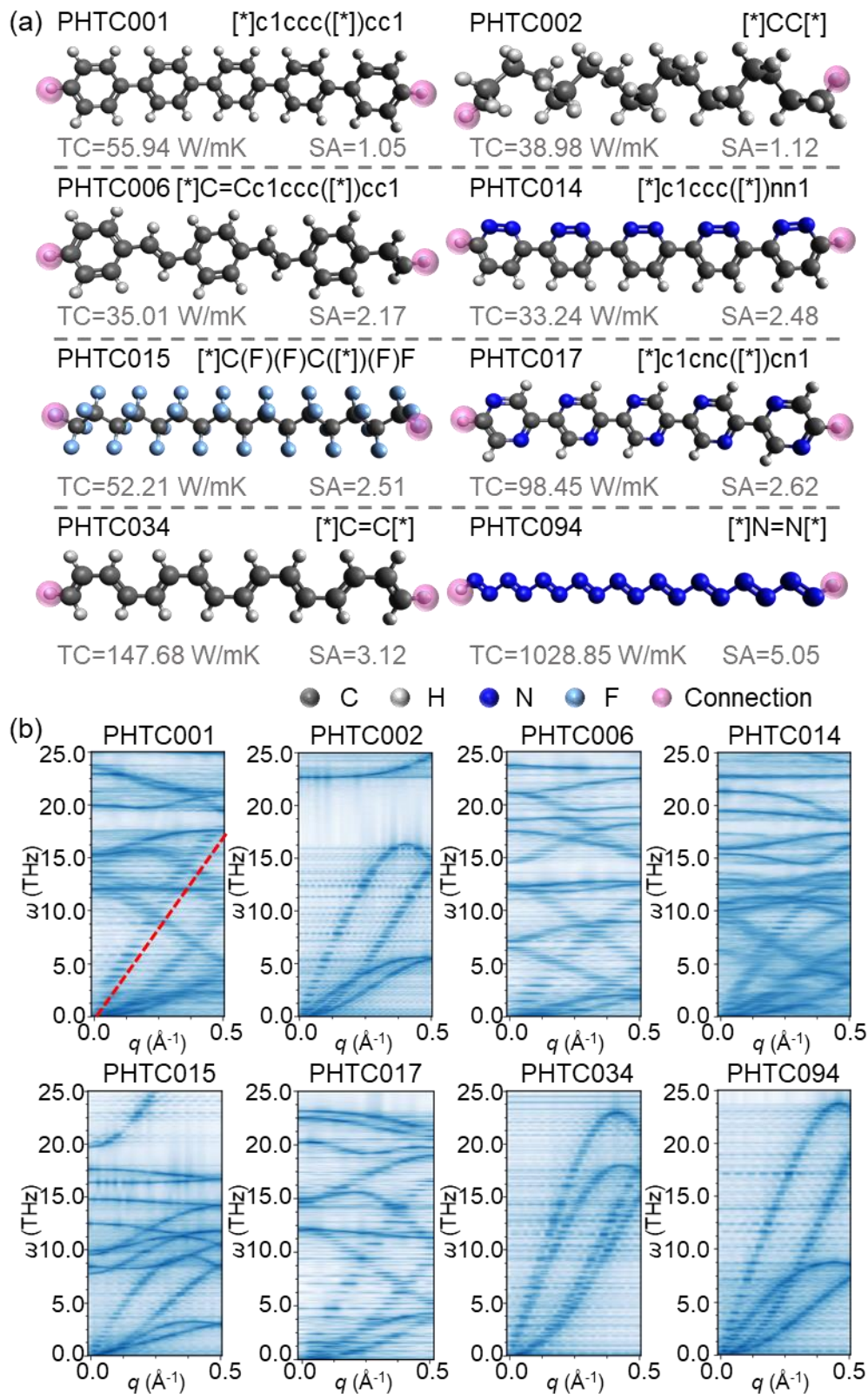


Fig. 7. Structure and phonon dispersion relations for the eight promising polymers. (a) Polymer chain structures. (b) Phonon dispersion relations. The q is wavevector, the ω is phonon frequency and the average phonon group velocity of one branch is estimated as the slope of the origin to the maximum frequency point as shown in the red dashed line in the PHTC001 structure.

Table 1. Volumetric heat capacity, phonon group velocity, phonon mean free path and phonon thermal conductivity for the eight promising polymers

Polymer ID	SMILES	SA	C_v (J/cm ³ K)	v_g (m/s)	l (nm)	k (W/mK)
PHTC001	[*]c1ccc([*])cc1	1.05	5.27	6822.21	1.55	55.94
PHTC002	[*]CC[*]	1.12	6.13	5240.91	1.21	38.98
PHTC006	[*]C=Cc1ccc([*])cc1	2.17	5.25	6295.54	1.06	35.01
PHTC014	[*]c1ccc([*])nn1	2.48	5.03	5927.05	1.12	33.24
PHTC015	[*]C(F)(F)C([*])(F)F	2.51	3.84	2952.11	4.61	52.21
PHTC017	[*]c1cnc([*])cn1	2.62	5.03	7439.50	2.63	98.45
PHTC034	[*]C=C[*]	3.12	4.37	8380.09	4.03	147.68
PHTC094	[*]N=N[*]	5.05	3.28	6378.73	49.22	1028.85

3. CONCLUSIONS

We have developed an interpretable ML framework for exploring high thermal conductivity polymer chains via high-throughput MD simulations. Inspired by the drug-like small molecule representation and the molecular force field, we reduced the initially calculated/collected 320 physical descriptors to 20 optimized descriptors by hierarchical down-selection. The constructed ML models are capable of effectively reflecting the relationship between optimized descriptors and property, and exhibit high accuracy in TC prediction. All the models of RF, XGBoost and MLP achieved the R^2 of more than 0.80, which is superior to that of represented by conventional graph descriptors. Moreover, the promotion or inhibition of TC by optimized descriptors like cross-sectional area and dihedral stiffness was captured by RF model using SHAP analysis.

Using the trained ML models, we discovered 107 promising polymers with TC greater than 20.00 W/mK, and 29 of which have SA scores no more than 3.00. These polymer structures have been validated through high-fidelity MD simulations. Further, we used SR with optimized descriptors to fit the TC of promising polymers, and the derived mathematical formulas enable a preliminary fast screening of high TC polymers without relying on ML models, which is friendly for experimental studies. In closing, we calculated phonon dispersion relations for eight typical polymer structures via phonon spectral energy density analysis to reveal the underlying TC mechanisms. Notably, most of these structures are π -conjugated polymers, whose overlapping p-orbitals enable easily to maintain strong chain stiffness and large group velocities. Our approach may assist in the research of high-

performance polymers that are not limited to TC.

4. METHODS

4.1 Polymer modeling and cross-sectional area calculation

Polymer modeling is a monomer to chain process, implemented in the STK tool, with input parameters of monomer SMILES and degree of polymerization⁷³. The length of the polymer chains was set uniformly to 50 nm, and the degree of polymerization was obtained by dividing the chain length by the monomer length and rounding up to an integer. Starting from the polymer SMILES, a molecular chain with polymerization degree 2 was generated by RDKit and optimized using the MMFF force field⁷⁴. Then, the monomer length was determined by measuring the distance between equivalent atoms in two repeating units in the heat transport direction. Following the modeling, a Python pipeline of PYSIMM realized the assignment of GAFF2 force field parameters and the generation of MD simulation input structure data files⁷⁵.

The cross-sectional area is one of the important parameters for thermal conductivity analysis. In molecular dynamics simulations, the calculation of the cross-sectional area is difficult for systems that do not occupy the entire simulation box. The cross-sectional area was estimated by the ratio of the van der Waals volume to the length of the monomer⁹. The Van der Waals volume of the monomer was calculated by the sum of atomic and bond contributions, and has been successfully tested and applied in previous drug compounds⁷⁶.

4.2 Calculation of TC by MD simulations

The TC of Polymer chains were obtained by non-equilibrium molecular dynamics simulations (NEMD) performed in a Large-scale Atomic/Molecular Massively Parallel Simulator (LAMMPS)⁷⁵. In terms of the NEMD method, the heat energy exchange was achieved by an enhanced version of the heat exchange algorithm, which rescales and shifts the velocities of particles inside reservoirs to impose a constant heat flux⁷⁷. The polymer chains were placed in a box of $540 \times 60 \times 60$ ($x \times y \times z$) Å box, where the dimension in the y and z directions was set to 60 Å to avoid interaction with the neighboring polymer chains. Before TC calculation, the polymer chain structures were relaxed to reach a stable conformation. Then, the polymer chain was divided into 50 slabs in the x direction, and the fixed regions at two ends of the chain were set as a heat-insulating walls. In the NEMD simulation, the system was run under NVT (constant number of atoms, volume, and temperature) and NVE (constant number of atoms,

volume, and energy) ensembles for 1 ns at 300 K sequentially to release chain stress^{30,78}. After that, the heat was added/extracted to the heat source/sink regions (20 Å of each region) at the end of the polymer chain in a regular rate to create a constant heat flux. The applied heat varies for different polymer chain structures and ranged from 0.01 eV/ps to 0.08 eV/ps. At last, the temperature profile was averaged over the last 2~3 ns and used for TC calculation based on Fourier's law $k = -J(d_T/d_x)$, where J is heat flux, d_T/d_x is the temperature gradient.

4.3 Descriptors calculation and ML models construction

The ideal polymer descriptors are required to minimize and completely represent polymer information, and is one of the key factors in determining the prediction accuracy of ML algorithms. The physical descriptors for this work were sourced from both Mordred software calculations and GAFF2 force field parameters extraction. The Mordred software was initially developed for small molecule characteristics in cheminformatics, which can calculate more than 1800 descriptors⁴¹. However, since we consider two linkages of polymer monomers, only 286 valid descriptors were obtained. Therefore, as a complement, we additionally extracted parameters from each polymer force field file as the descriptor. For graph descriptors, MACCS, Morgan and cMorgan fingerprints were calculated in the RDKit package³⁹. The Mol2vec fingerprints were embedded via Mol2vec³⁴. We referred the polymer representation model trained using PoLyInfo and PIIM databases⁵⁴.

The ML models of RF, XGBoost and MLP were implemented by using Scikit-learn⁷⁹. Hyperparametric optimization for RF, XGBoost and MLP was operated with the Bayesian Optimization package⁸⁰ which is a global optimization tool to achieve good prediction accuracy R^2 . The Gaussian regression process and acquisition function with 10 randomly pairs of parameters were selected for initial training, and the ideal parameters for each ML model were determined after 100 optimization iterations⁴⁶.

To explain the association of optimized descriptors with TC, we used the SHAP toolkit with RF model to evaluate the feature importance⁵⁶. The SHAP analysis is based on a game-theoretic approach that associates the optimal credit allocation with the local explanations of the model, which considers the model performance by neglecting each feature and provides direction of each descriptor effect⁴⁶.

4.4 Mathematical formulas for TC fitted by symbolic regression (SR)

The mathematical formulae were acquired and selected using an efficient stepwise strategy with SR based on genetic programming (GPSR) as implemented in gplearn⁶⁸. The 107 polymer structures

with TC greater than 20.00 W/mK were randomly divided into 3:1 as training and test sets respectively. At first, Pearson coefficients were used as evaluation metrics of training fitness to filter optimized descriptors and generate sub-descriptors, and a new dataset containing 22 descriptors was generated. Further, the grid search strategy with the hyperparameters and metric R^2 as listed in Table 2 was applied to determine the mathematical formulas. We ultimately discussed four formulas at Pareto front were identified by Latin hypercube sampling approach ^{70,71}. More information about SR can be found in the Supplementary Section S9.

Table 2. Setup of hyperparameters in gplearn for GPSR

Parameter	Value
Generations	300
Population size in every generation	5000
Probability of crossover (pc)	[0.30,0.90], step=0.05
Subtree mutation (ps)	[(1-pc)/3,(1-pc)/2] (step= 0.01)
Hoist mutation (ph)	[(1-pc)/3,(1-pc)/2] (step = 0.01)
Point mutation (pp)	1-pc-ps-ph
Function set	{+, -, ×, ÷, \sqrt{x} , $\ln x$, $ x $, $-x$, $1/x$ }
Parsimony coefficient	0.001, 0.003, 0.005
Metric	R^2
Stopping criterial	0.900
Random_state	0, 1, 2, 3, 4
Init_depth	[2, 6], [4, 8], [6, 10], [2, 10]

4.5 Analysis of phonon dispersion relations by phonon spectral energy density (Phonon-SED)

To understand the TC mechanism of polymers, MD simulations coupled with Phonon-SED approach ⁷² were employed to calculate the dispersion relations of polymers. The polymer chain with a length of 100 Å was constructed as an input of SMILES and placed into a box with the cross section of 60×60 Å. After energy minimization, the system was run under the NVT (constant number of atoms, volume, and temperature) ensemble for 0.25 ns at 2 K sequentially to release chain stress. Subsequently, the system was run under the NVE (constant number of atoms, volume, and energy) ensemble for 2 million steps with the timestep of 0.25 fs. During this period, the velocity and position of each atom in the polymer backbone were recorded with intervals of 20 steps. The Phonon-SED converted the time domain information of atomic velocities and positions into wave vectors versus angular frequencies via two-dimensional Fourier transform, expressed as

$$\Phi(q, \omega) = \frac{1}{4\pi\tau_0 N_T} \sum_{\alpha}^{\{x,y,z\}} \sum_b^B m_b \left| \int_0^{\tau_0} \sum_n^{N_T} \dot{u}_\alpha(n, b; t) \times e^{iq \cdot r(n,0;t) - i\omega t} dt \right|^2 \quad (1)$$

Where q is the wavevector, ω is the frequency, τ_0 is the simulation time, m_b is the mass of atom b , α is the cartesian direction, N_T is the number of the unit cell in the polymer chain, $\dot{u}_\alpha(n, b; t)$ is the velocity of atom b in the unit cell n at time t in the α direction, and $r(n, 0; t)$ is the equilibrium position of unit cell n .

Acknowledgements

This work was supported by Shanghai Pujiang Program (No. 20PJ1407500), the National Natural Science Foundation of China (No. 52006134), Shanghai Key Fundamental Research Grant (No. 21JC1403300), SJTU-Warwick Joint Seed Fund. The computations in this paper were run on the π 2.0 cluster supported by the Center for High Performance Computing at Shanghai Jiao Tong University.

Author Contributions

Conceptualization: S. J.

Methodology: X. H., S. M. and S. J.

Investigation: X. H., S. M. and S. J.

Supervision: S. J., C. Y. Z. and H. W.

Writing—original draft: X. H., S. M. and S. J.

Writing—review & editing: X. H., S. M., S. J., C. Y. Z. and H. W.

Competing interests

Authors declare that they have no competing interests.

Supporting Information

The supporting information is available free of charge.

REFERENCES

- 1 Zhang, B. *et al.* Modulating Thermal Transport in Polymers and Interfaces: Theories, Simulations, and Experiments. *ES Energy & Environment* **5**, 37-55, doi:10.30919/eseec8c306 (2019).
- 2 Ghaffari-Mosanenzadeh, S. *et al.* A review on high thermally conductive polymeric composites.

- Polymer Composites* **43**, 692-711, doi:<https://doi.org/10.1002/pc.26420> (2022).
- 3 Qian, X., Zhou, J. & Chen, G. Phonon-engineered extreme thermal conductivity materials. *Nature Materials* **20**, 1188-1202, doi:10.1038/s41563-021-00918-3 (2021).
- 4 Guo, Y., Zhou, Y. & Xu, Y. Engineering polymers with metal-like thermal conductivity—Present status and future perspectives. *Polymer* **233**, 124168, doi:<https://doi.org/10.1016/j.polymer.2021.124168> (2021).
- 5 Ma, H. & Tian, Z. Effects of polymer topology and morphology on thermal transport: A molecular dynamics study of bottlebrush polymers. *Applied Physics Letters* **110**, 091903, doi:10.1063/1.4976946 (2017).
- 6 Xu, Y. *et al.* Nanostructured polymer films with metal-like thermal conductivity. *Nature Communications* **10**, 1771, doi:10.1038/s41467-019-09697-7 (2019).
- 7 Ma, J. *et al.* Thermal conductivity of electrospun polyethylene nanofibers. *Nanoscale* **7**, 16899-16908, doi:10.1039/C5NR04995D (2015).
- 8 Singh, V. *et al.* High thermal conductivity of chain-oriented amorphous polythiophene. *Nature Nanotechnology* **9**, 384-390, doi:10.1038/nnano.2014.44 (2014).
- 9 Liu, X., Lin, C. & Rao, Z. Thermal conductivity of straight-chain polytetrafluoroethylene: A molecular dynamics study. *International Journal of Thermal Sciences* **159**, 106646, doi:<https://doi.org/10.1016/j.ijthermalsci.2020.106646> (2021).
- 10 Crnjar, A., Melis, C. & Colombo, L. Assessing the anomalous superdiffusive heat transport in a single one-dimensional PEDOT chain. *Physical Review Materials* **2**, 015603, doi:10.1103/PhysRevMaterials.2.015603 (2018).
- 11 Henry, A. & Chen, G. High Thermal Conductivity of Single Polyethylene Chains Using Molecular Dynamics Simulations. *Physical Review Letters* **101**, 235502, doi:10.1103/PhysRevLett.101.235502 (2008).
- 12 Zhang, T., Wu, X. & Luo, T. Polymer Nanofibers with Outstanding Thermal Conductivity and Thermal Stability: Fundamental Linkage between Molecular Characteristics and Macroscopic Thermal Properties. *The Journal of Physical Chemistry C* **118**, 21148-21159, doi:10.1021/jp5051639 (2014).
- 13 Liu, J. & Yang, R. Length-dependent thermal conductivity of single extended polymer chains. *Physical Review B* **86**, 104307, doi:10.1103/PhysRevB.86.104307 (2012).
- 14 Zhang, T. & Luo, T. Morphology-influenced thermal conductivity of polyethylene single chains

- and crystalline fibers. *Journal of Applied Physics* **112**, 094304, doi:10.1063/1.4759293 (2012).
- 15 Liu, J., Ju, S., Ding, Y. & Yang, R. Size effect on the thermal conductivity of ultrathin polystyrene films. *Applied Physics Letters* **104**, 153110, doi:10.1063/1.4871737 (2014).
- 16 Kim, S. *et al.* PubChem Substance and Compound databases. *Nucleic Acids Research* **44**, D1202-D1213, doi:10.1093/nar/gkv951 (2015).
- 17 Yang, J., Tao, L., He, J., McCutcheon, J. R. & Li, Y. Machine learning enables interpretable discovery of innovative polymers for gas separation membranes. *Science Advances* **8**, eabn9545, doi:doi:10.1126/sciadv.abn9545 (2022).
- 18 Chen, L. *et al.* Polymer informatics: Current status and critical next steps. *Materials Science and Engineering: R: Reports* **144**, 100595, doi:<https://doi.org/10.1016/j.mser.2020.100595> (2021).
- 19 Ramprasad, R., Batra, R., Pilania, G., Mannodi-Kanakkithodi, A. & Kim, C. Machine learning in materials informatics: recent applications and prospects. *npj Computational Materials* **3**, 54, doi:10.1038/s41524-017-0056-5 (2017).
- 20 Wu, S., Yamada, H., Hayashi, Y., Zamengo, M. & Yoshida, R. Potentials and challenges of polymer informatics: exploiting machine learning for polymer design. *arXiv preprint arXiv:2010.07683* (2020).
- 21 Audus, D. J. & de Pablo, J. J. Polymer Informatics: Opportunities and Challenges. *ACS Macro Letters* **6**, 1078-1082, doi:10.1021/acsmacrolett.7b00228 (2017).
- 22 Huang, Y. *et al.* Structure–Property Correlation Study for Organic Photovoltaic Polymer Materials Using Data Science Approach. *The Journal of Physical Chemistry C* **124**, 12871-12882, doi:10.1021/acs.jpcc.0c00517 (2020).
- 23 Nagasawa, S., Al-Naamani, E. & Saeki, A. Computer-Aided Screening of Conjugated Polymers for Organic Solar Cell: Classification by Random Forest. *The Journal of Physical Chemistry Letters* **9**, 2639-2646, doi:10.1021/acs.jpcclett.8b00635 (2018).
- 24 Afzal, M. A. F., Haghightlari, M., Ganesh, S. P., Cheng, C. & Hachmann, J. Accelerated Discovery of High-Refractive-Index Polyimides via First-Principles Molecular Modeling, Virtual High-Throughput Screening, and Data Mining. *The Journal of Physical Chemistry C* **123**, 14610-14618, doi:10.1021/acs.jpcc.9b01147 (2019).
- 25 Wu, C. *et al.* Flexible Temperature-Invariant Polymer Dielectrics with Large Bandgap. *Advanced Materials* **32**, 2000499, doi:<https://doi.org/10.1002/adma.202000499> (2020).

- 26 Wu, K. *et al.* Prediction of polymer properties using infinite chain descriptors (ICD) and machine learning: Toward optimized dielectric polymeric materials. *Journal of Polymer Science Part B: Polymer Physics* **54**, 2082-2091, doi:<https://doi.org/10.1002/polb.24117> (2016).
- 27 Sahu, H. *et al.* An Informatics Approach for Designing Conducting Polymers. *ACS Applied Materials & Interfaces* **13**, 53314-53322, doi:10.1021/acsami.1c04017 (2021).
- 28 Tao, L., Varshney, V. & Li, Y. Benchmarking Machine Learning Models for Polymer Informatics: An Example of Glass Transition Temperature. *Journal of Chemical Information and Modeling* **61**, 5395-5413, doi:10.1021/acs.jcim.1c01031 (2021).
- 29 Bhowmik, R., Sihh, S., Pachter, R. & Vernon, J. P. Prediction of the specific heat of polymers from experimental data and machine learning methods. *Polymer* **220**, 123558, doi:<https://doi.org/10.1016/j.polymer.2021.123558> (2021).
- 30 Zhu, M.-X., Song, H.-G., Yu, Q.-C., Chen, J.-M. & Zhang, H.-Y. Machine-learning-driven discovery of polymers molecular structures with high thermal conductivity. *International Journal of Heat and Mass Transfer* **162**, 120381, doi:<https://doi.org/10.1016/j.ijheatmasstransfer.2020.120381> (2020).
- 31 Ma, R., Zhang, H. & Luo, T. Exploring High Thermal Conductivity Amorphous Polymers Using Reinforcement Learning. *ACS Applied Materials & Interfaces* **14**, 15587-15598, doi:10.1021/acsami.1c23610 (2022).
- 32 Wu, S. *et al.* Machine-learning-assisted discovery of polymers with high thermal conductivity using a molecular design algorithm. *npj Computational Materials* **5**, 66, doi:10.1038/s41524-019-0203-2 (2019).
- 33 Zhou, T., Wu, Z., Chilukoti, H. K. & Müller-Plathe, F. Sequence-Engineering Polyethylene-Polypropylene Copolymers with High Thermal Conductivity Using a Molecular-Dynamics-Based Genetic Algorithm. *Journal of Chemical Theory and Computation* **17**, 3772-3782, doi:10.1021/acs.jctc.1c00134 (2021).
- 34 Jaeger, S., Fulle, S. & Turk, S. Mol2vec: Unsupervised Machine Learning Approach with Chemical Intuition. *Journal of Chemical Information and Modeling* **58**, 27-35, doi:10.1021/acs.jcim.7b00616 (2018).
- 35 Morgan, H. L. The generation of a unique machine description for chemical structures—a technique developed at chemical abstracts service. *Journal of chemical documentation* **5**, 107-113 (1965).

- 36 Durant, J. L., Leland, B. A., Henry, D. R. & Nourse, J. G. Reoptimization of MDL Keys for Use in Drug Discovery. *Journal of Chemical Information and Computer Sciences* **42**, 1273-1280, doi:10.1021/ci010132r (2002).
- 37 Capecchi, A., Probst, D. & Reymond, J.-L. One molecular fingerprint to rule them all: drugs, biomolecules, and the metabolome. *Journal of Cheminformatics* **12**, 43, doi:10.1186/s13321-020-00445-4 (2020).
- 38 D'Souza, S., Prema, K. V. & Balaji, S. Machine learning models for drug–target interactions: current knowledge and future directions. *Drug Discovery Today* **25**, 748-756, doi:<https://doi.org/10.1016/j.drudis.2020.03.003> (2020).
- 39 Landrum, G. RDKit: A software suite for cheminformatics, computational chemistry, and predictive modeling. *Greg Landrum* (2013).
- 40 Karelson, M., Lobanov, V. S. & Katritzky, A. R. Quantum-Chemical Descriptors in QSAR/QSPR Studies. *Chemical Reviews* **96**, 1027-1044, doi:10.1021/cr950202r (1996).
- 41 Moriwaki, H., Tian, Y.-S., Kawashita, N. & Takagi, T. Mordred: a molecular descriptor calculator. *Journal of Cheminformatics* **10**, 4, doi:10.1186/s13321-018-0258-y (2018).
- 42 Haghighatlari, M. *et al.* ChemML: A machine learning and informatics program package for the analysis, mining, and modeling of chemical and materials data. *WIREs Computational Molecular Science* **10**, e1458, doi:<https://doi.org/10.1002/wcms.1458> (2020).
- 43 Mauri, A., Consonni, V., Pavan, M. & Todeschini, R. Dragon software: An easy approach to molecular descriptor calculations. *Match* **56**, 237-248 (2006).
- 44 Roy, K. & Das, R. N. QSTR with extended topochemical atom (ETA) indices. 16. Development of predictive classification and regression models for toxicity of ionic liquids towards *Daphnia magna*. *Journal of Hazardous Materials* **254-255**, 166-178, doi:<https://doi.org/10.1016/j.jhazmat.2013.03.023> (2013).
- 45 Shields, B. J. *et al.* Bayesian reaction optimization as a tool for chemical synthesis. *Nature* **590**, 89-96, doi:10.1038/s41586-021-03213-y (2021).
- 46 Tiihonen, A. *et al.* Predicting Antimicrobial Activity of Conjugated Oligoelectrolyte Molecules via Machine Learning. *Journal of the American Chemical Society* **143**, 18917-18931, doi:10.1021/jacs.1c05055 (2021).
- 47 Domingos, P. A few useful things to know about machine learning. *Communications of the ACM* **55**, 78-87 (2012).

- 48 Marchetti, F., Moroni, E., Pandini, A. & Colombo, G. Machine Learning Prediction of Allosteric Drug Activity from Molecular Dynamics. *The Journal of Physical Chemistry Letters* **12**, 3724-3732, doi:10.1021/acs.jpcclett.1c00045 (2021).
- 49 Schober, P., Boer, C. & Schwarte, L. A. Correlation coefficients: appropriate use and interpretation. *Anesthesia & Analgesia* **126**, 1763-1768 (2018).
- 50 Chandrashekar, G. & Sahin, F. A survey on feature selection methods. *Computers & Electrical Engineering* **40**, 16-28, doi:<https://doi.org/10.1016/j.compeleceng.2013.11.024> (2014).
- 51 Kuenneth, C. *et al.* Polymer informatics with multi-task learning. *Patterns* **2**, 100238, doi:<https://doi.org/10.1016/j.patter.2021.100238> (2021).
- 52 Kamal, D. *et al.* Novel high voltage polymer insulators using computational and data-driven techniques. *The Journal of Chemical Physics* **154**, 174906, doi:10.1063/5.0044306 (2021).
- 53 Otsuka, S., Kuwajima, I., Hosoya, J., Xu, Y. & Yamazaki, M. in *2011 International Conference on Emerging Intelligent Data and Web Technologies.* 22-29 (IEEE).
- 54 Ma, R. & Luo, T. PI1M: A Benchmark Database for Polymer Informatics. *Journal of Chemical Information and Modeling*, doi:10.1021/acs.jcim.0c00726 (2020).
- 55 Wang, J., Wolf, R. M., Caldwell, J. W., Kollman, P. A. & Case, D. A. Development and testing of a general amber force field. *Journal of Computational Chemistry* **25**, 1157-1174, doi:<https://doi.org/10.1002/jcc.20035> (2004).
- 56 Lundberg, S. M. & Lee, S.-I. A unified approach to interpreting model predictions. *Advances in neural information processing systems* **30** (2017).
- 57 Hayashi, Y., Shiomi, J., Morikawa, J. & Yoshida, R. RadonPy: Automated Physical Property Calculation using All-atom Classical Molecular Dynamics Simulations for Polymer Informatics. *arXiv preprint arXiv:2203.14090* (2022).
- 58 McInnes, L., Healy, J. & Melville, J. Umap: Uniform manifold approximation and projection for dimension reduction. *arXiv preprint arXiv:1802.03426* (2018).
- 59 Kavzoglu, T. & Mather, P. M. The role of feature selection in artificial neural network applications. *International Journal of Remote Sensing* **23**, 2919-2937, doi:10.1080/01431160110107743 (2002).
- 60 Ma, H. & Tian, Z. Chain rotation significantly reduces thermal conductivity of single-chain polymers. *Journal of Materials Research* **34**, 126-133, doi:10.1557/jmr.2018.362 (2019).
- 61 Hua, C., Lindsay, L., Chen, X. & Minnich, A. J. Generalized Fourier's law for nondiffusive

- thermal transport: Theory and experiment. *Physical Review B* **100**, 085203, doi:10.1103/PhysRevB.100.085203 (2019).
- 62 Robbins, A. B. & Minnich, A. J. Crystalline polymers with exceptionally low thermal conductivity studied using molecular dynamics. *Applied Physics Letters* **107**, 201908, doi:10.1063/1.4936195 (2015).
- 63 Zhang, T. & Luo, T. Role of Chain Morphology and Stiffness in Thermal Conductivity of Amorphous Polymers. *The Journal of Physical Chemistry B* **120**, 803-812, doi:10.1021/acs.jpcc.5b09955 (2016).
- 64 Ertl, P. & Schuffenhauer, A. Estimation of synthetic accessibility score of drug-like molecules based on molecular complexity and fragment contributions. *Journal of Cheminformatics* **1**, 8, doi:10.1186/1758-2946-1-8 (2009).
- 65 Weng, B. *et al.* Simple descriptor derived from symbolic regression accelerating the discovery of new perovskite catalysts. *Nature Communications* **11**, 3513, doi:10.1038/s41467-020-17263-9 (2020).
- 66 Wang, Y., Wagner, N. & Rondinelli, J. M. Symbolic regression in materials science. *MRS Communications* **9**, 793-805, doi:10.1557/mrc.2019.85 (2019).
- 67 Vladislavleva, E. Y. *Model-based problem solving through symbolic regression via pareto genetic programming*. (CentER, Tilburg University Tilburg, 2008).
- 68 Stephens, T. *Genetic Programming in Python, with a scikit-learn inspired API: gplearn*, (2022).
- 69 Zhou, Y., Rao, Y., Zhang, L., Ju, S. & Wang, H. Machine-learning prediction of Vegard's law factor and volume size factor for binary substitutional metallic solid solutions. *Acta Materialia* **237**, 118166, doi:<https://doi.org/10.1016/j.actamat.2022.118166> (2022).
- 70 Paulson, N. H., Libera, J. A. & Stan, M. Flame spray pyrolysis optimization via statistics and machine learning. *Materials & Design* **196**, 108972, doi:<https://doi.org/10.1016/j.matdes.2020.108972> (2020).
- 71 Agarwal, G., Doan, H. A., Robertson, L. A., Zhang, L. & Assary, R. S. Discovery of Energy Storage Molecular Materials Using Quantum Chemistry-Guided Multiobjective Bayesian Optimization. *Chemistry of Materials* **33**, 8133-8144, doi:10.1021/acs.chemmater.1c02040 (2021).
- 72 Thomas, J. A., Turney, J. E., Iutzi, R. M., Amon, C. H. & McGaughey, A. J. H. Predicting phonon dispersion relations and lifetimes from the spectral energy density. *Physical Review B*

- 81**, 081411, doi:10.1103/PhysRevB.81.081411 (2010).
- 73 Turcani, L., Berardo, E. & Jelfs, K. E. stk: A python toolkit for supramolecular assembly. *Journal of Computational Chemistry* **39**, 1931-1942, doi:<https://doi.org/10.1002/jcc.25377> (2018).
- 74 Tosco, P., Stiefl, N. & Landrum, G. Bringing the MMFF force field to the RDKit: implementation and validation. *Journal of Cheminformatics* **6**, 37, doi:10.1186/s13321-014-0037-3 (2014).
- 75 Fortunato, M. E. & Colina, C. M. pysimm: A python package for simulation of molecular systems. *SoftwareX* **6**, 7-12, doi:<https://doi.org/10.1016/j.softx.2016.12.002> (2017).
- 76 Zhao, Y. H., Abraham, M. H. & Zissimos, A. M. Fast Calculation of van der Waals Volume as a Sum of Atomic and Bond Contributions and Its Application to Drug Compounds. *The Journal of Organic Chemistry* **68**, 7368-7373, doi:10.1021/jo034808o (2003).
- 77 Wirnsberger, P., Frenkel, D. & Dellago, C. An enhanced version of the heat exchange algorithm with excellent energy conservation properties. *The Journal of Chemical Physics* **143**, 124104, doi:10.1063/1.4931597 (2015).
- 78 Ju, S., Palpant, B. & Chalopin, Y. Adverse Effects of Polymer Coating on Heat Transport at the Solid–Liquid Interface. *The Journal of Physical Chemistry C* **121**, 13474-13480, doi:10.1021/acs.jpcc.7b02123 (2017).
- 79 Pedregosa, F. *et al.* Scikit-learn: Machine learning in Python. *the Journal of machine Learning research* **12**, 2825-2830 (2011).
- 80 Nogueira, F. Bayesian Optimization: Open source constrained global optimization tool for Python. URL <https://github.com/fmfn/BayesianOptimization> (2014).

Supplemental Materials for

Exploring High Thermal Conductivity Polymers via Interpretable Machine Learning with Physical Descriptors

Xiang Huang^{1,†}, Shengluo Ma^{1,†}, C. Y. Zhao¹, Hong Wang², and Shenghong Ju^{1,2,*}

¹ China-UK Low Carbon College, Shanghai Jiao Tong University, Shanghai, China

² Materials Genome Initiative Center, School of Material Science and Engineering, Shanghai Jiao Tong University, Shanghai, China

†Equal contribution

* Corresponding author: shenghong.ju@sjtu.edu.cn.

Section S1. Downselection of polymer descriptors

Polymer descriptors were downselected in three stages: removing features with low variance (Var.), primary filtering referred to different correlation coefficients (Cor.), and final selection assisted with ML model (Opt.), as shown in Fig. S1.

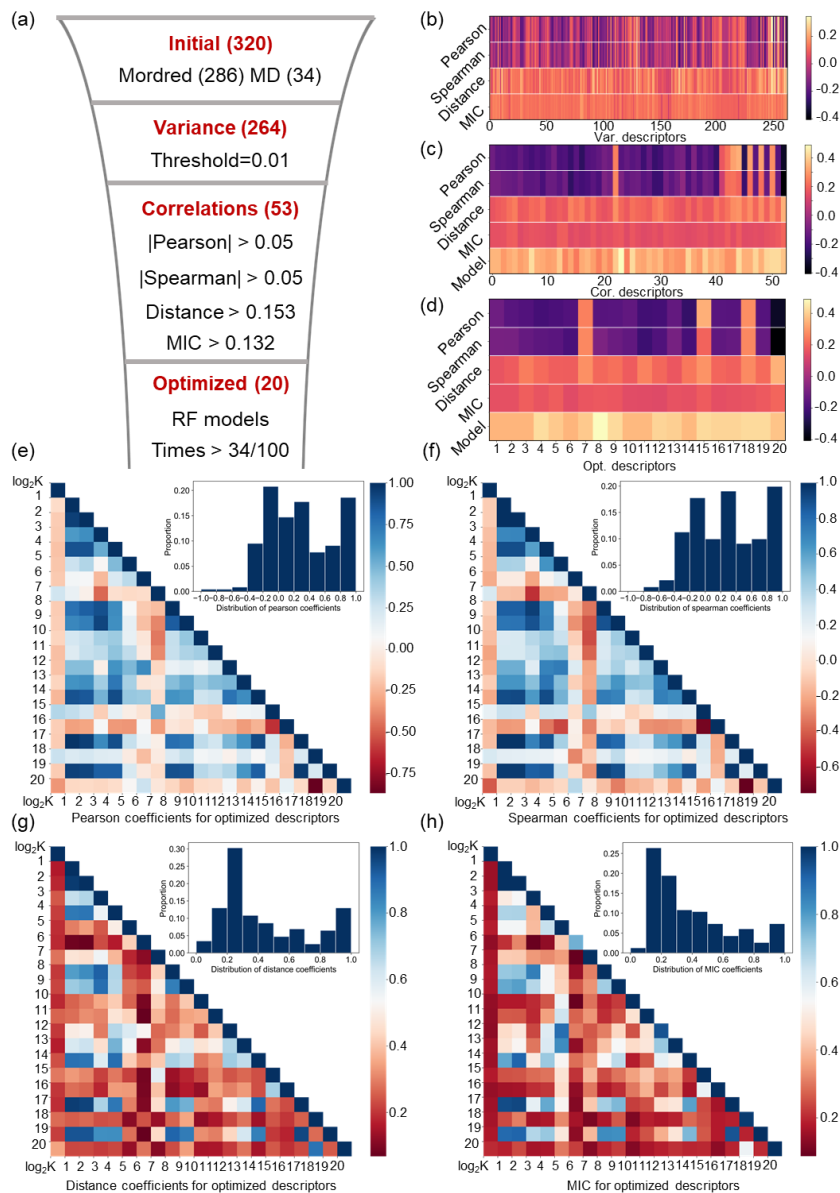


Fig. S1. Downselection and analysis of descriptors. (a) Process of descriptors downselection. (b), (c) and (d) Relationship between descriptors at different stages (Var., Cor. and Opt.) and thermal conductivity based on various metrics or frequency of occurrence of descriptors through 100 Random Forest (RF) model selections. (e), (f), (g) and (h) Pearson, Spearman, Distance and MIC correlation matrices showing correlations among optimized descriptors and TC. The inset shows the distribution statistics of the corresponding correlation coefficient values respectively. The description of the 20 optimized descriptors is available in Section S3.

Section S2. List of MD-inspired and Mordred-based fingerprints

The MD-inspired descriptors include force field related (FF-related) descriptors and thermal conductivity related (TC-related) descriptors, listed in Table S1.

Table S1. Descriptions of all MD-inspired descriptors

Name	Description
Epsilon_max	Maximum value of the depth of the energy potential (Lennard–Jones parameter)
Epsilon_min	Minimum value of the depth of the energy potential (Lennard–Jones parameter)
Epsilon_average	Average value of the depth of the energy potential (Lennard–Jones parameter)
Sigma_max	Maximum value of the equilibrium distance (Lennard–Jones parameter)
Sigma_min	Minimum value of the equilibrium distance (Lennard–Jones parameter)
Sigma_average	Average value of the equilibrium distance (Lennard–Jones parameter)
Kb_max	Maximum value of force constants of the bond
Kb_min	Minimum value of force constants of the bond
Kb_average	Average value of force constants of the bond
R0_max	Maximum value of equilibration structural parameters of the bond
R0_min	Minimum value of equilibration structural parameters of the bond
R0_average	Average value of equilibration structural parameters of the bond
Ka_max	Maximum value of force constants of the bond angle
Ka_min	Minimum value of force constants of the bond angle
Ka_average	Average value of force constants of the bond angle
Theta0_max	Maximum value of equilibration structural parameters of the bond angle
Theta0_min	Minimum value of equilibration structural parameters of the bond angle
Theta0_average	Average value of equilibration structural parameters of the bond angle
Kd_max	Maximum value of force constants of the dihedral angle
Kd_min	Minimum value of force constants of the dihedral angle
Kd_average	Average value of force constants of the dihedral angle
Nd_max	Maximum value of multiplicity for the torsional angle parameters
Nd_min	Minimum value of multiplicity for the torsional angle parameters
Nd_average	Average value of multiplicity for the torsional angle parameters
Delta_max	Maximum value of phase angle for the torsional angle parameters
Delta_min	Minimum value of phase angle for the torsional angle parameters
Delta_average	Average value of phase angle for the torsional angle parameters
Ki_max	Maximum value of force constants of the improper angle
Ki_min	Minimum value of force constants of the improper angle
Ki_average	Average value of force constants of the improper angle
MW	Molecular weight of monomer
MW_ratio	The ratio of the molecular weight of the main chain to that of the monomer
Vdw	Van der Waals volume of the monomer
Cross-sectional	Equivalent cross-sectional area of polymer chain

The Mordred-based descriptors were calculated by Mordred software ¹, the 286 Mordred-based descriptors in this work are listed in Table S2, and the detailed meaning could be found at <https://mordred-descriptor.github.io/documentation/master/descriptors.html> (accessed Aug 10, 2022).

Table S2. Descriptions of 286 Mordred-based descriptors

ABC	nAcid	nBase	SpMax_A	SpMAD_A
LogEE_A	VE1_A	VR1_A	VR3_A	nAromAtom
nAtom	nBridgehead	nHetero	nH	nN
nO	nS	nF	nCl	nBr
ATS0dv	ATS0Z	AATS0dv	AATS0d	AATS2d
AATS0Z	AATS1Z	AATS2Z	AATS3Z	ATSC0dv
ATSC1dv	ATSC2dv	ATSC3dv	ATSC4dv	ATSC5dv
ATSC6dv	ATSC7dv	ATSC8dv	ATSC1d	ATSC2d
ATSC3d	ATSC4d	ATSC5d	ATSC6d	ATSC7d
ATSC8d	ATSC0Z	ATSC1Z	ATSC2Z	ATSC3Z
ATSC4Z	ATSC5Z	ATSC6Z	ATSC7Z	ATSC8Z
AATSC0dv	AATSC1dv	AATSC2dv	AATSC3dv	AATSC0d
AATSC1d	AATSC2d	AATSC3d	AATSC0Z	AATSC1Z
AATSC2Z	AATSC3Z	MATS1dv	MATS2dv	MATS3dv
MATS1d	MATS2d	MATS3d	MATS1Z	MATS2Z
MATS3Z	GATS1dv	GATS2dv	GATS3dv	GATS1d
GATS2d	GATS3d	GATS1Z	GATS2Z	GATS3Z
BCUTdv-1h	BCUTdv-1l	BCUTd-1h	BCUTd-1l	BCUTZ-1h
BCUTZ-1l	BalabanJ	BertzCT	nBondsD	nBondsT
C1SP1	C2SP1	C1SP2	C3SP2	C1SP3
C2SP3	C3SP3	C4SP3	HybRatio	Xch-4d
Xch-5d	Xch-6d	Xch-4dv	Xc-3d	Xc-4d
Xc-5d	Xc-6d	Xpc-4d	AXp-0d	AXp-1d
AXp-2d	AXp-3d	NsCH3	NdCH2	NssCH2
NdsCH	NsssCH	NddC	NdssC	NaaaC
NssssC	NsNH2	NssNH	NaaNH	NdsN
NaaN	NsssN	NaasN	NsOH	NdO
NssO	NaaO	NdS	NssS	NaaS
NddssS	SsssCH	SdssC	SaasC	SaaaC
SsssN	SaasN	AETA_beta	AETA_beta_s	ETA_beta_ns_d
AETA_beta_ns_d	AETA_eta_RL	AETA_eta_BR	ETA_epsilon_3	ETA_dBeta
fragCpx	fMF	nHBAcc	IC0	IC1
IC2	IC3	SIC0	SIC1	SIC2
SIC3	SIC4	BIC5	CIC0	MIC0
MIC1	MIC2	Kier2	Kier3	FilterItLogS
PEOE_VSA1	PEOE_VSA2	PEOE_VSA3	PEOE_VSA4	PEOE_VSA6
PEOE_VSA7	PEOE_VSA8	PEOE_VSA9	PEOE_VSA10	PEOE_VSA11
PEOE_VSA12	PEOE_VSA13	SMR_VSA1	SMR_VSA3	SMR_VSA4
SMR_VSA6	SMR_VSA9	SlogP_VSA1	SlogP_VSA2	SlogP_VSA3

SlogP_VSA4	SlogP_VSA5	SlogP_VSA7	SlogP_VSA8	SlogP_VSA10
SlogP_VSA11	EState_VSA1	EState_VSA2	EState_VSA3	EState_VSA4
EState_VSA5	EState_VSA6	EState_VSA7	EState_VSA8	EState_VSA9
EState_VSA10	VSA_EState1	VSA_EState2	VSA_EState3	VSA_EState4
VSA_EState5	VSA_EState7	VSA_EState8	VSA_EState9	AMID_h
AMID_N	AMID_O	AMID_X	nRing	n5Ring
n6Ring	n7Ring	nHRing	n4HRing	n5HRing
n6HRing	n5aRing	naHRing	n6aHRing	nARing
n5ARing	n6ARing	nAHRing	n5AHRing	n6AHRing
nFRing	n7FRing	n8FRing	n9FRing	n10FRing
n11FRing	n12FRing	nG12FRing	nFHRing	n7FHRing
n8FHRing	n10FHRing	nG12FHRing	nFaRing	n8FaRing
n9FaRing	n10FaRing	nG12FaRing	nFaHRing	nFARing
n10FARing	n12FARing	nG12FARing	nFAHRing	nG12FAHRing
RotRatio	SLogP	TopoPSA(NO)	TopoPSA	GGI4
GGI5	GGI6	GGI7	JGI1	JGI2
JGI3	JGI4	JGI5	JGI6	JGI7
JGI8	JGI9	JGI10	JGT10	TopoShapeIndex
mZagreb1				

Section S3. Descriptions of optimized descriptors for polymer thermal conductivity (TC) prediction

Polymer optimized descriptors were obtained by downselection, listed in Table S3.

Table S3. Descriptions of all MD-inspired descriptors

No.	Name	Description	Block
1	ABC	Atom-bond connectivity index	Atom-bond connectivity index descriptor
2	LogEE_A	LogEE of adjacency matrix	Adjacency matrix descriptor
3	Nh	Number of H atoms	Atom count descriptor
4	ATSC0dv	Centered moreau-broto autocorrelation of lag 0 weighted by valence electrons	Centered Autocorrelation of Topological Structure descriptor
5	BCUTdv-1h	First heighest eigenvalue of Burden matrix weighted by valence electrons	BCUT descriptor
6	Xc-4d	4-ordered Chi cluster weighted by sigma electrons	Chi descriptor
7	ETA_dBeta	ETA delta beta	ETA delta beta descriptor
8	CIC0	0-ordered complementary information content	Complementary information content descriptor
9	Kier2	kappa shape index 2	Kappa shape index 2 descriptor
10	SMR_VSA6	MOE MR VSA Descriptor 6 ($2.75 \leq x < 3.05$)	MOE type descriptors using Wildman-Crippen MR and surface area contribution
11	SlogP_VSA3	MOE logP VSA Descriptor 3 ($-0.20 \leq x < 0.00$)	MOE type descriptors using Wildman-Crippen LogP and surface area contribution
12	EState_VSA10	EState VSA Descriptor 10 ($9.17 \leq x < 15.00$)	MOE type descriptors using EState indices and surface area contribution
13	TopoPSA(NO)	Topological polar surface area (use only nitrogen and oxygen)	Topological polar surface area descriptor
14	mZagreb1	modified Zagreb index (version 1)	Zagreb index descriptor
15	Kd_average	Average value of force constants of the dihedral angle	FF-related descriptor
16	Nd_average	Average value of multiplicity for the torsional angle parameters	FF-related descriptor
17	MW	Molecular weight of monomer	TC- related descriptor
18	MW_ratio	The ratio of the molecular weight of the main chain to that of the monomer	TC- related descriptor
19	Vdw	Van der Waals volume of the monomer	TC- related descriptor
20	Cross-sectional	Equivalent cross-sectional area of polymer chain	TC- related descriptor

Section S4. Construction of different ML models with optimized descriptors

Figure S2 shows the RF, XGBoost and MLP models trained with the optimized descriptors. The test set is consisted of 100 randomly selected polymer structures from the benchmark dataset.

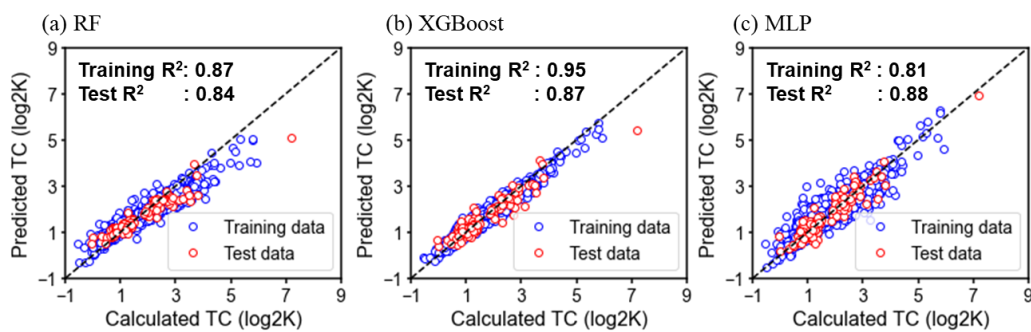


Fig. S2. Construction of different ML models with optimized descriptors

Section S5. Accuracy of ML models at different descriptors downselection stages

Figure S3 shows the accuracy of ML models at different descriptors downselection stages. The extra principal component analysis (PCA)² technique with 95% variance was used to compare.

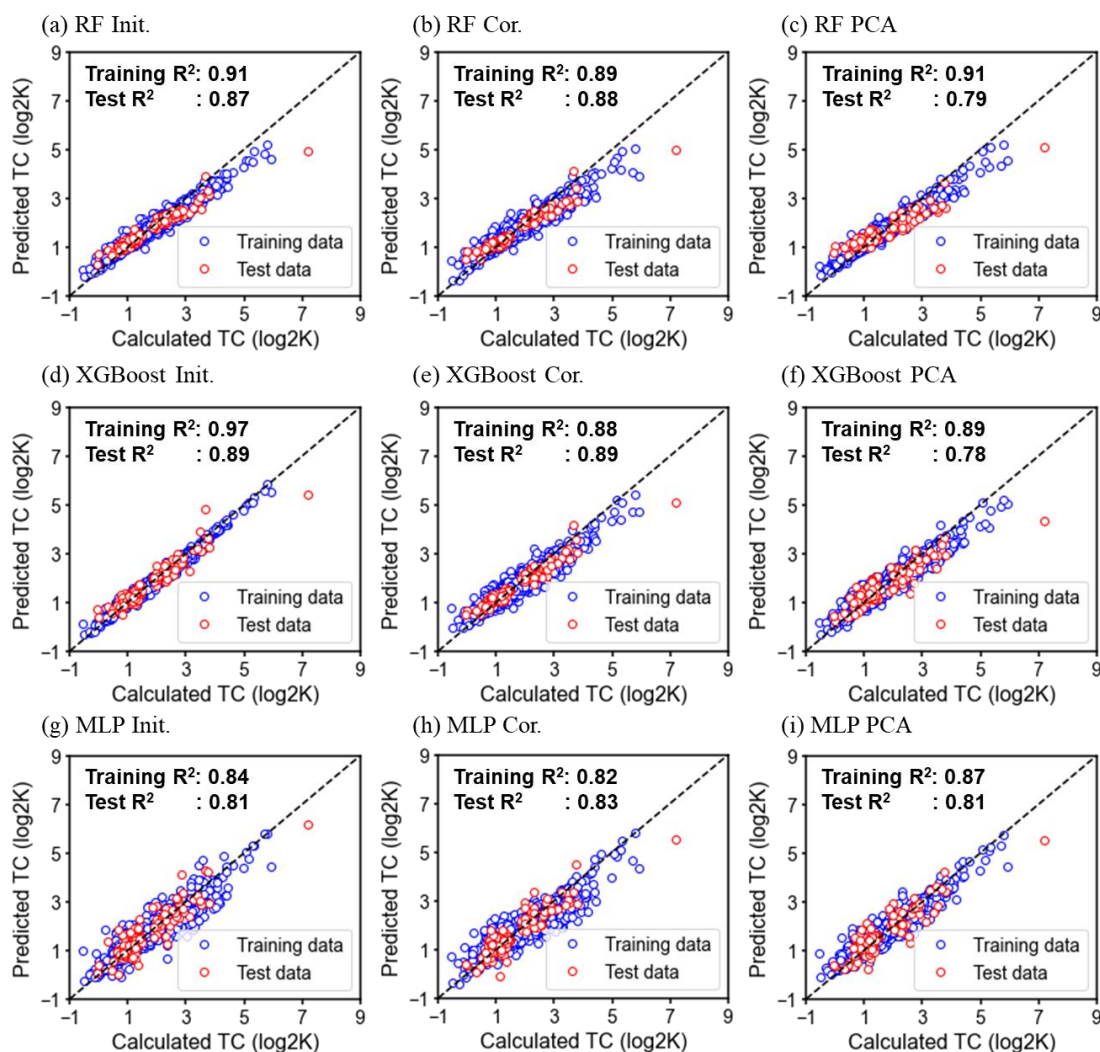


Fig. S3. Accuracy of ML models at different descriptors downselection stages

Figure S4 represents the relationship between the number of principal components and cumulative variance. Here, the PCA with 19 principal components of 95% variance was performed.

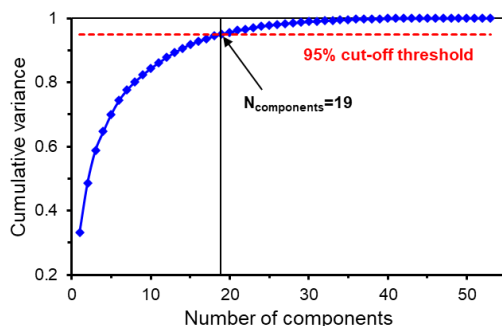


Fig. S4. Relationship between the number of principal components and cumulative variance

Section S6. Accuracy of ML models with various graph descriptors

Figure S5 shows the training and testing accuracy of ML models using Mol2vec ³, MACCS ⁴, Morgan and Morgan count (cMorgan) ⁵ graph descriptors.

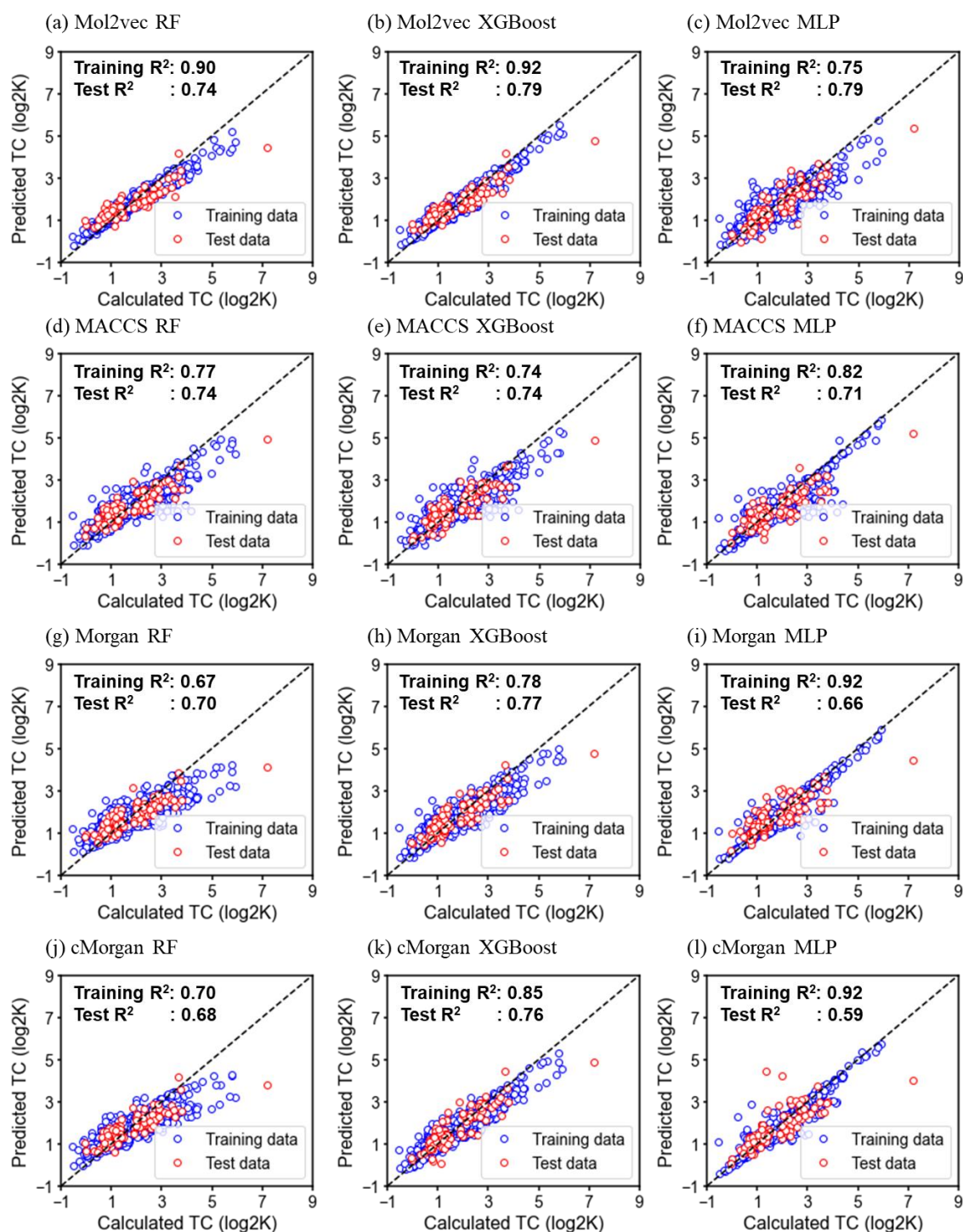


Fig. S5. Accuracy of ML models with various graph descriptors

Section S7. Analysis of the feature importance

Figure S6 exhibits the SHAP values⁶ for each optimized descriptor of the training data set polymers as a function of corresponding descriptor value. The subplots are sorted by the average SHAP value. The SHAP values of the top-ranked features corresponding to the training dataset polymers show a monotonic relationship with the feature values overall, while the lower-ranked features have difficulty in capturing this rule. Wherein, the relationships between two important MD-inspired descriptors and TC are shown in Fig. S7.

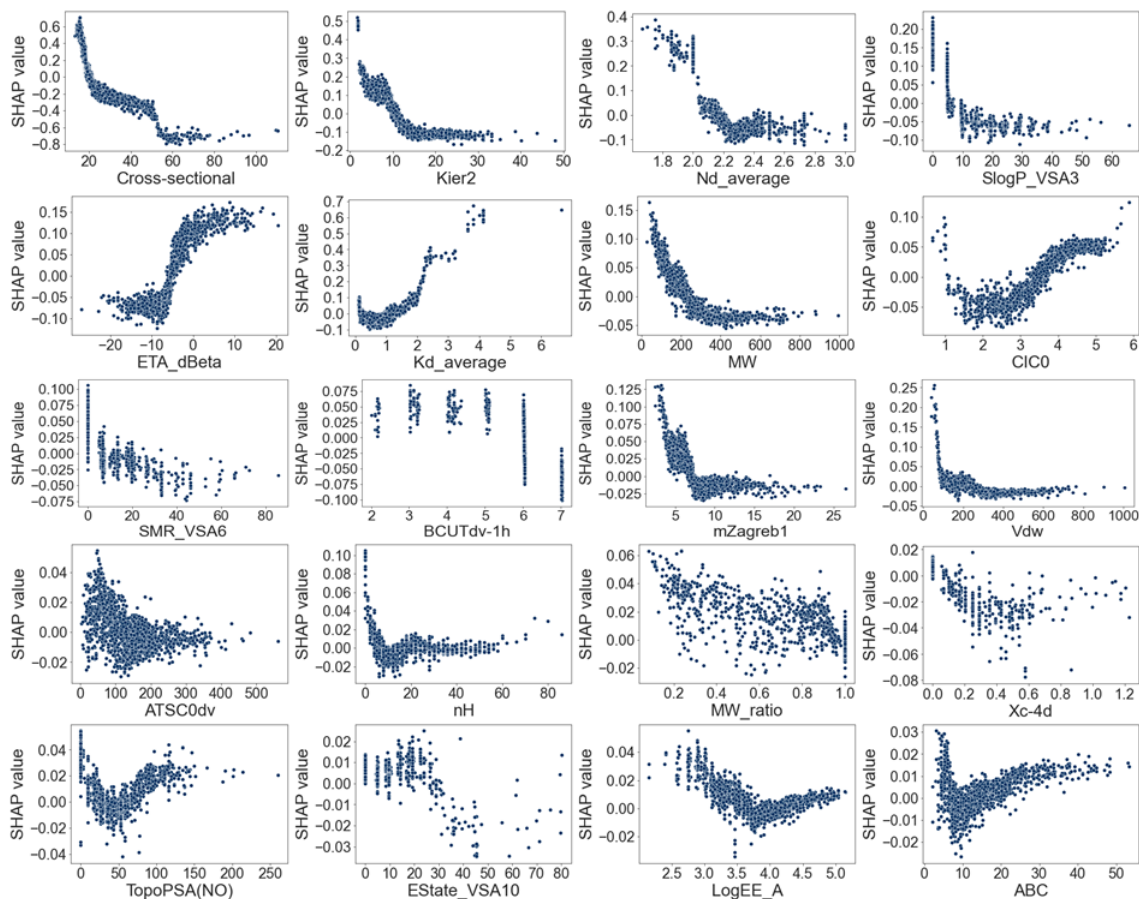


Fig. S6. Distribution of SHAP values for each optimized descriptor

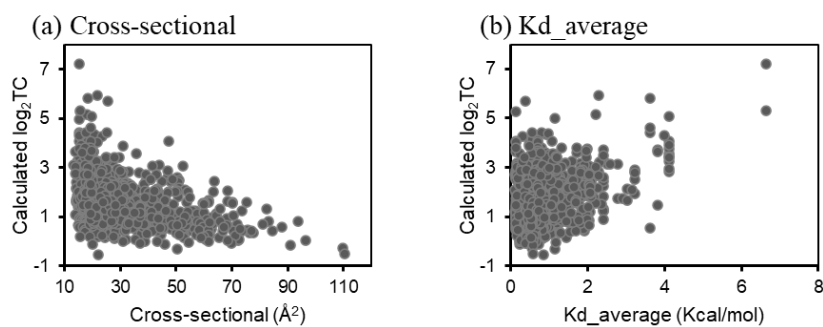


Fig. S7. Relationships between two important MD-inspired descriptors and TC of 1735 benchmark polymers.

Section S8. Discovery of polymers with high thermal conductivity (PHTC) by proposed ML workflow

We performed virtual screening of polymer data in PolyInfo and PIIM based on the trained RF, XGBoost and MLP machine learning models, respectively. In this work, totally of 107 polymer structures with TC greater than 20 W/mK were identified and validated by MD simulations, which are listed in Table S3. In this work, a total of 107 polymer structures with thermal conductivity greater than 20 W/mK were identified and validated by molecular dynamics simulations, as listed in Table 4, and the relevant monomer structure can be viewed in Figure S8 by polymer ID (PID). The TC obtained from RF, XGBoost and MLP model predictions and MD simulations are \log_2 TC in W/mK. The effective cross-sectional area of the polymer is given in \AA^2 .

Table S4. MD-validated polymer structures with thermal conductivity greater than 20 W/mK

PID	SMILES	SA score	Cross- sectional	RF	XGBoost	MLP	MD
PHTC001	[*]c1ccc([*])cc1	1.05	18.32	5.00	5.77	6.28	5.81
PHTC002	[*]CC[*]	1.12	15.69	3.91	4.66	5.30	5.28
PHTC003	[*]c1cccc([*])c1	1.50	20.74	4.02	5.21	5.86	4.59
PHTC004	[*]CC(=O)N[*]	2.07	15.13	4.00	4.34	4.05	4.41
PHTC005	[*]c1cccc([*])n1	2.15	19.72	4.65	4.98	5.65	5.06
PHTC006	[*]C=Cc1ccc([*])cc1	2.17	16.76	4.29	4.36	5.48	5.13
PHTC007	[*]c1ccc2cc([*])ccc2c1	2.17	18.28	3.55	4.37	5.01	5.12
PHTC008	[*]CC(=O)O[*]	2.21	15.09	4.01	4.45	4.36	4.98
PHTC009	[*]c1cccc2c([*])cccc12	2.22	23.86	3.17	3.81	4.36	4.35
PHTC010	[*]c1ccc([*])c(Cl)c1	2.23	21.89	3.73	4.06	5.34	4.61
PHTC011	[*]c1ccc2ccc([*])cc2c1	2.28	19.21	3.81	4.49	5.05	4.62
PHTC012	[*]OCC([*])=O	2.28	20.86	3.31	4.17	3.70	4.33
PHTC013	[*]c1ccc([*])nc1	2.33	16.98	4.85	5.08	5.45	4.50
PHTC014	[*]c1ccc([*])nn1	2.48	15.68	4.87	5.91	4.97	5.05
PHTC015	[*]C(F)(F)C([*])(F)F	2.51	25.57	4.05	5.27	5.07	5.71
PHTC016	[*]NC(=O)N[*]	2.57	14.34	4.53	4.91	3.76	5.47
PHTC017	[*]c1cnc([*])cn1	2.62	15.75	5.11	6.08	5.85	6.62
PHTC018	[*]c1ccc2nc([*])ccc2n1	2.64	16.79	3.96	4.00	5.62	5.93
PHTC019	[*]Oc1ccc([*])nc1	2.65	14.79	4.16	4.46	4.17	4.43
PHTC020	[*]Oc1ccc([*])cn1	2.65	14.74	4.16	4.52	4.17	4.76
PHTC021	[*]c1ccc2nc([*])ccc2c1	2.78	17.62	3.96	4.19	5.59	4.38
PHTC022	[*]c1cncc([*])n1	2.80	18.06	5.08	5.84	5.53	4.34
PHTC023	[*]c1ccnc([*])n1	2.82	18.06	5.08	5.82	5.52	5.00
PHTC024	[*]NNC([*])=O	2.86	14.28	4.19	4.56	3.32	4.83

PID	SMILES	SA score	Cross- sectional	RF	XGBoost	MLP	MD
PHTC025	[*]c1csc([*])n1	2.87	15.82	5.11	6.20	5.76	5.75
PHTC026	[*]c1cnc2cc([*])ccc2c1	2.91	17.29	3.99	4.24	5.63	4.82
PHTC027	[*]c1ccc2oc([*])nc2c1	2.97	15.17	3.91	3.55	3.59	4.34
PHTC028	[*]c1ccc(-c2ccc([*])s2)s1	3.00	15.98	4.06	4.26	4.22	5.64
PHTC029	[*]C=Cc1ccc([*])c(F)c1	3.04	17.60	3.89	4.34	4.80	4.41
PHTC030	[*]C=C/C=C/[*]	3.07	15.68	5.06	5.35	5.79	5.33
PHTC031	[*]C=C/C=C/[*]	3.07	14.06	5.05	5.10	5.97	7.55
PHTC032	[*]/C=C/C=C/[*]	3.07	14.26	5.05	5.10	5.95	6.91
PHTC033	[*]c1nc([*])nc(Cl)n1	3.09	13.85	4.53	5.64	5.63	6.51
PHTC034	[*]C=C[*]	3.12	15.35	5.08	5.44	6.92	7.21
PHTC035	[*]C=C/C=C/C=C/[*]	3.20	13.73	4.65	4.34	4.86	7.42
PHTC036	[*]/C=C/C=C/C=C/[*]	3.20	13.60	4.65	4.34	4.87	7.31
PHTC037	[*]c1nnc([*])s1	3.27	8.76	5.09	6.04	6.14	5.75
PHTC038	[*]CCOC(=O)NCCNC(=O)O[*]	3.33	15.55	3.20	4.10	3.65	4.38
PHTC039	[*]C(=O)c1cnc([*])cn1	3.34	15.80	4.11	4.34	4.35	4.54
PHTC040	[*]c1cnc([*])s1	3.35	15.34	4.86	5.77	5.40	4.95
PHTC041	[*]C1=Cc2ccc([*])cc21	3.37	18.78	4.37	4.64	5.50	5.11
PHTC042	[*]OC(=O)O[*]	3.38	11.93	3.97	4.05	3.96	5.61
PHTC043	[*]c1ccc2nc([*])ncc2n1	3.39	15.82	3.98	3.95	5.54	5.83
PHTC044	[*]c1cc(Cl)c([*])nn1	3.45	19.29	4.19	5.08	4.97	4.52
PHTC045	[*]c1cnc([*])nn1	3.49	14.33	5.06	5.97	5.57	6.46
PHTC046	[*]c1nnc([*])c(Cl)c1Cl	3.51	15.39	4.11	5.12	5.41	4.60
PHTC047	[*]c1cnnc([*])n1	3.53	16.38	5.04	5.92	5.33	5.60
PHTC048	[*]c1cnc([*])n1C	3.55	19.00	4.25	4.46	5.63	4.49
PHTC049	[*]c1ccc(-c2nnc([*])s2)s1	3.63	14.53	4.15	4.39	4.83	5.39
PHTC050	[*]c1nnc([*])c(F)c1F	3.64	12.41	4.40	5.32	4.51	4.75
PHTC051	[*]c1ccc(-c2cnc([*])s2)s1	3.76	15.25	4.17	4.44	4.85	5.51
PHTC052	[*]C(Cl)=C([*])Cl	3.86	20.41	4.17	4.38	4.81	5.13
PHTC053	[*]/C(Cl)=C(/[*)Cl	3.86	20.56	4.13	4.42	4.80	5.08
PHTC054	[*]C#C[*]	3.87	5.85	4.23	4.58	5.15	9.63
PHTC055	[*]C1=CC=C1[*]	3.90	22.30	4.36	5.72	5.65	4.62
PHTC056	[*]c1nnc([*])c(O)n1	3.90	16.45	4.50	5.18	4.20	4.96
PHTC057	[*]c1noc([*])c1Br	3.90	11.67	4.61	5.55	4.77	4.97
PHTC058	[*]C(=O)N1C(=O)N([*])C1=O	4.04	16.85	3.66	4.36	5.49	5.37
PHTC059	[*]NC(=O)C(=S)C([*])=O	4.08	21.85	4.01	5.07	4.60	5.91
PHTC060	[*]C(=O)c1nnc([*])nn1	4.09	11.89	4.36	5.35	4.15	5.95
PHTC061	[*]c1cc2nc([*])sc2nn1	4.09	14.51	4.38	4.81	5.11	4.35
PHTC062	[*]C(=O)C([*])=S	4.20	16.81	3.78	4.92	4.41	5.03
PHTC063	[*]C1=C(F)C(Cl)=C1[*]	4.28	17.13	4.69	4.59	5.00	5.84

PID	SMILES	SA score	Cross- sectional	RF	XGBoost	MLP	MD
PHTC064	[*]C1=CC=C2C([*])=CC=C12	4.32	22.02	3.94	3.73	4.63	6.16
PHTC065	[*]NC(=O)C([*])=N	4.32	18.67	3.86	5.17	3.12	4.37
PHTC066	[*]SC([*])=O	4.34	8.22	4.70	5.29	4.52	6.73
PHTC067	[*]/C=C/C=C([*])Cl	4.36	17.41	4.65	3.72	4.63	5.90
PHTC068	[*]/C(F)=C([*])C#N	4.36	20.54	3.77	5.11	3.47	6.02
PHTC069	[*]C=Cc1csc(-c2cc([*])cs2)c1	4.45	15.88	3.69	3.61	3.08	4.33
PHTC070	[*]/C=C/C=C/C=C([*])Cl	4.45	15.96	4.28	4.78	3.99	5.66
PHTC071	[*]/C=C/C=C/C=C([*])Cl	4.45	15.96	4.28	4.78	3.99	5.66
PHTC072	[*]/C(F)=C([*])Cl	4.46	18.39	4.44	5.10	4.90	6.18
PHTC073	[*]C(F)=C([*])Cl	4.46	17.50	4.69	5.25	4.94	5.83
PHTC074	[*]OC([*])=S	4.53	14.49	4.63	5.07	3.76	5.20
PHTC075	[*]C#CC=C[*]	4.54	18.03	4.51	5.02	5.18	5.16
PHTC076	[*]OC([*])=C	4.54	19.19	4.07	4.36	3.57	4.55
PHTC077	[*]/C=C([*])Cl	4.55	21.62	4.28	4.80	5.14	6.03
PHTC078	[*]C=C([*])C#N	4.58	24.93	3.53	4.00	2.70	4.88
PHTC079	[*]C(=S)C(=O)C(F)(F)C([*])(F)F	4.59	25.30	3.19	4.28	3.92	4.41
PHTC080	[*]SS[*]	4.66	13.04	3.77	3.91	0.95	4.93
PHTC081	[*]/C=C/C=C/C=C([*])N	4.66	15.44	4.20	4.41	4.69	5.53
PHTC082	[*]NNC([*])=N	4.67	15.08	4.45	4.61	4.41	4.51
PHTC083	[*]C1=CC2=NC([*])=CC2=N1	4.75	17.77	4.55	4.07	4.51	6.10
PHTC084	[*]C#CC#CC=C[*]	4.78	12.75	4.11	3.79	4.61	5.99
PHTC085	[*]C=C([*])F	4.82	17.93	4.71	5.35	4.81	6.64
PHTC086	[*]/C=C/N[*]	4.83	15.68	5.02	5.28	6.52	5.44
PHTC087	[*]C#C/C(C#N)=C([*])C#N	4.88	15.14	3.46	5.00	4.71	5.37
PHTC088	[*]/N=C/C(=S)N[*]	4.88	18.77	4.37	4.29	5.00	5.06
PHTC089	[*]/N=N/C([*])=O	4.90	8.82	4.55	5.76	6.04	7.35
PHTC090	[*]/C=C/O[*]	4.92	15.71	3.94	3.83	3.43	4.60
PHTC091	[*]=CC=NN=[*]	4.98	5.95	4.69	4.92	7.53	4.71
PHTC092	[*]NN[*]	5.00	11.88	4.79	5.37	6.33	4.60
PHTC093	[*]/N=N/[*]	5.05	5.21	4.83	5.95	6.81	10.38
PHTC094	[*]N=N[*]	5.05	5.93	4.83	5.95	6.76	10.01
PHTC095	[*]/N=C([*])Cl	5.08	9.62	5.06	5.71	6.50	6.98
PHTC096	[*]C#C/C(C#N)=C([*])Cl	5.14	14.06	3.63	5.06	4.58	5.79
PHTC097	[*]/C=N/C=C([*])C	5.14	17.30	4.02	3.64	4.36	4.72
PHTC098	[*]/C=C/C=CS[*]	5.17	14.14	4.14	3.28	4.13	4.36
PHTC099	[*]C1=CC2=CC([*])=NC2=N1	5.28	17.50	4.62	4.10	4.55	5.79
PHTC100	[*]/C=C/N=C([*])Cl	5.38	19.65	4.16	4.37	4.61	5.60
PHTC101	[*]/C=C/S[*]	5.44	14.40	4.57	4.20	5.74	4.35
PHTC102	[*]/C=N/[*]	5.53	14.02	5.10	6.07	6.07	6.82

PID	SMILES	SA	Cross-	RF	XGBoost	MLP	MD
		score	sectional				
PHTC103	<chem>[*]/N=N/N=C(/[*])C#N</chem>	5.66	11.24	3.69	5.07	4.33	6.68
PHTC104	<chem>[*]/C=N/C=C/C=C(/[*])Cl</chem>	5.70	15.50	4.33	4.46	4.07	5.70
PHTC105	<chem>[*]/C=C(/[*])[O-]</chem>	5.73	18.54	4.07	4.66	2.87	6.10
PHTC106	<chem>[*]/C=C/C=C/N=N/[*]</chem>	5.76	12.71	4.74	4.11	7.01	6.59
PHTC107	<chem>[*]C([2H])=C([*])[2H]</chem>	7.27	11.30	4.32	4.33	1.07	7.48

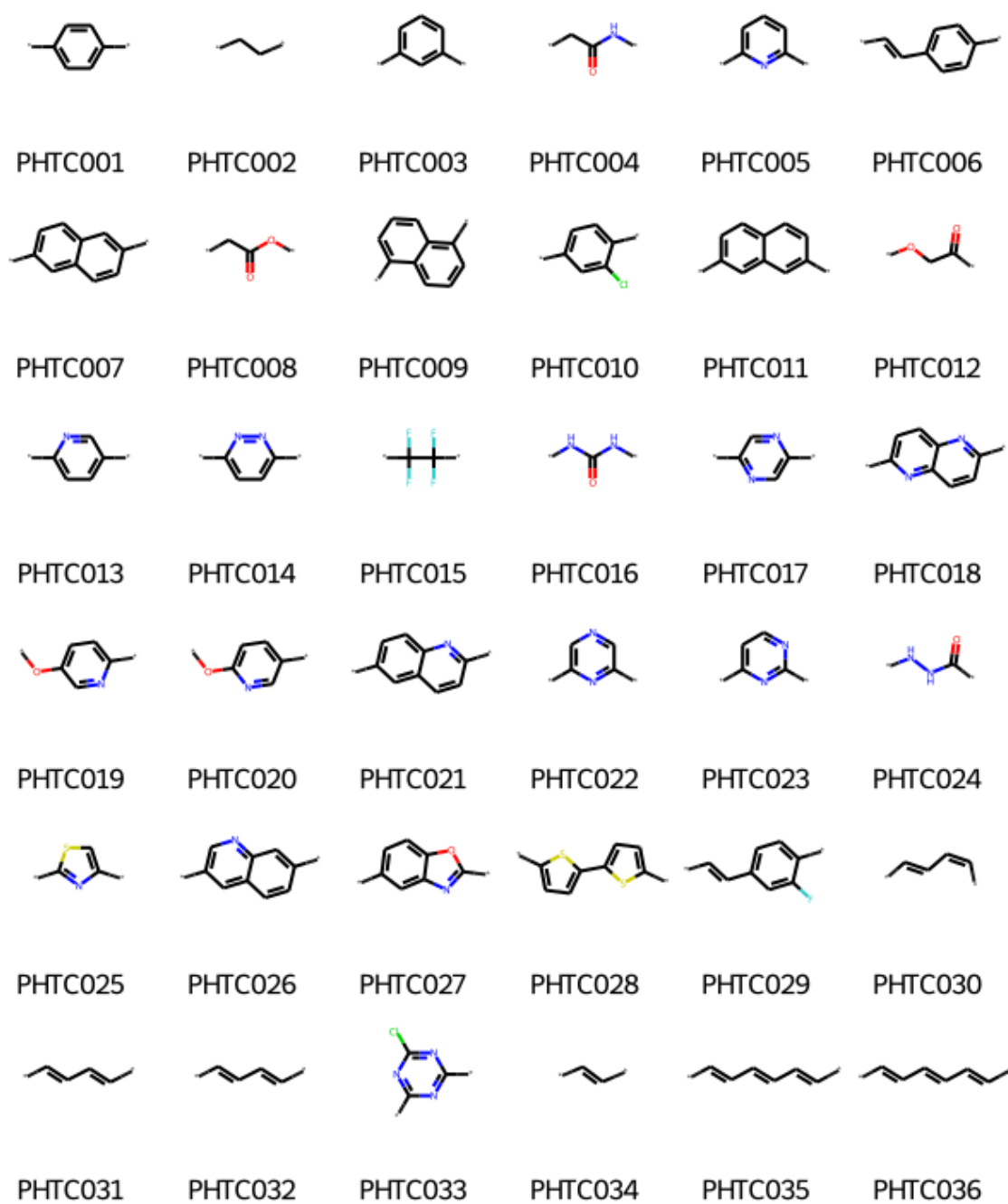


Fig. S8. Continued

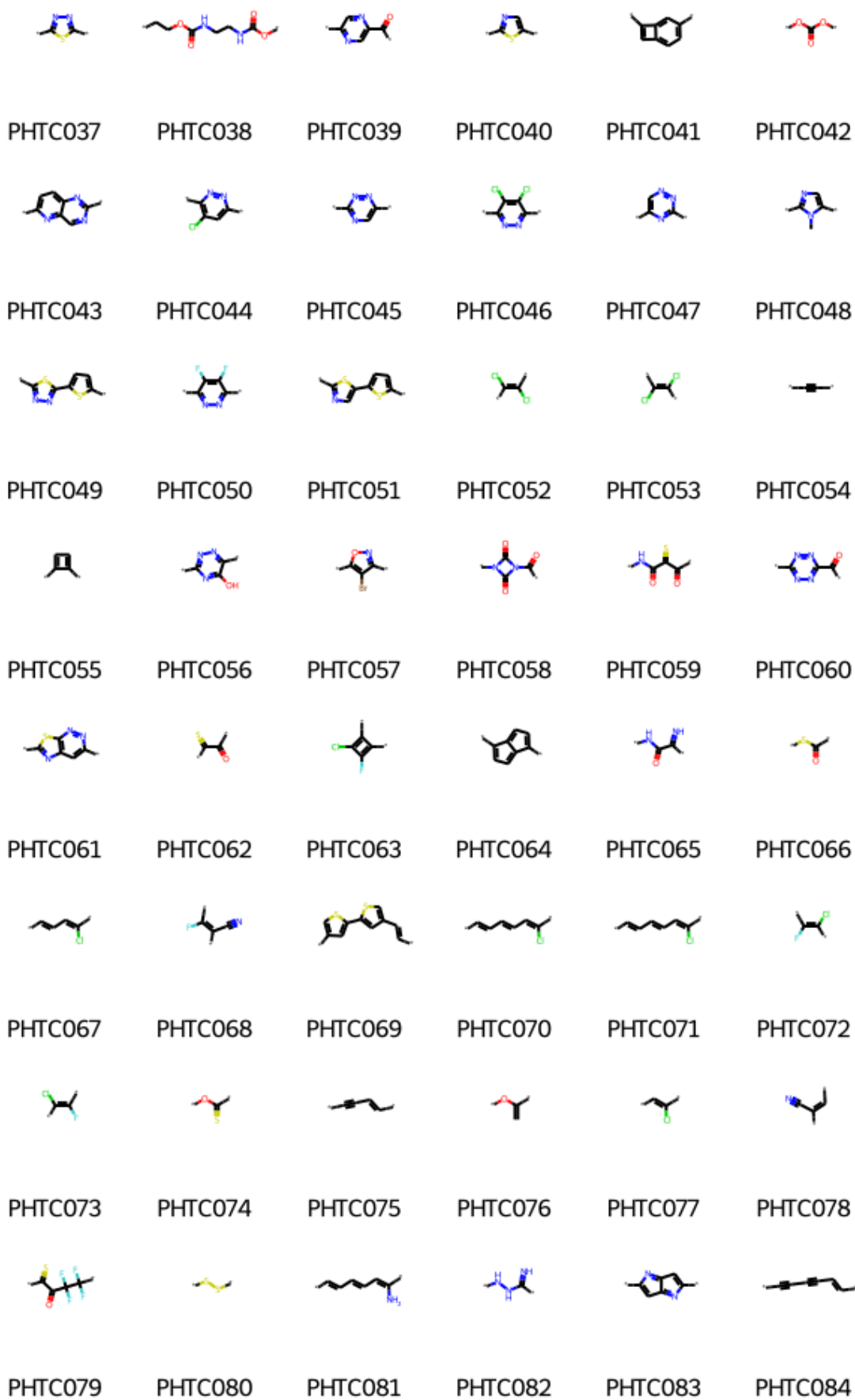


Fig. S8. Continued

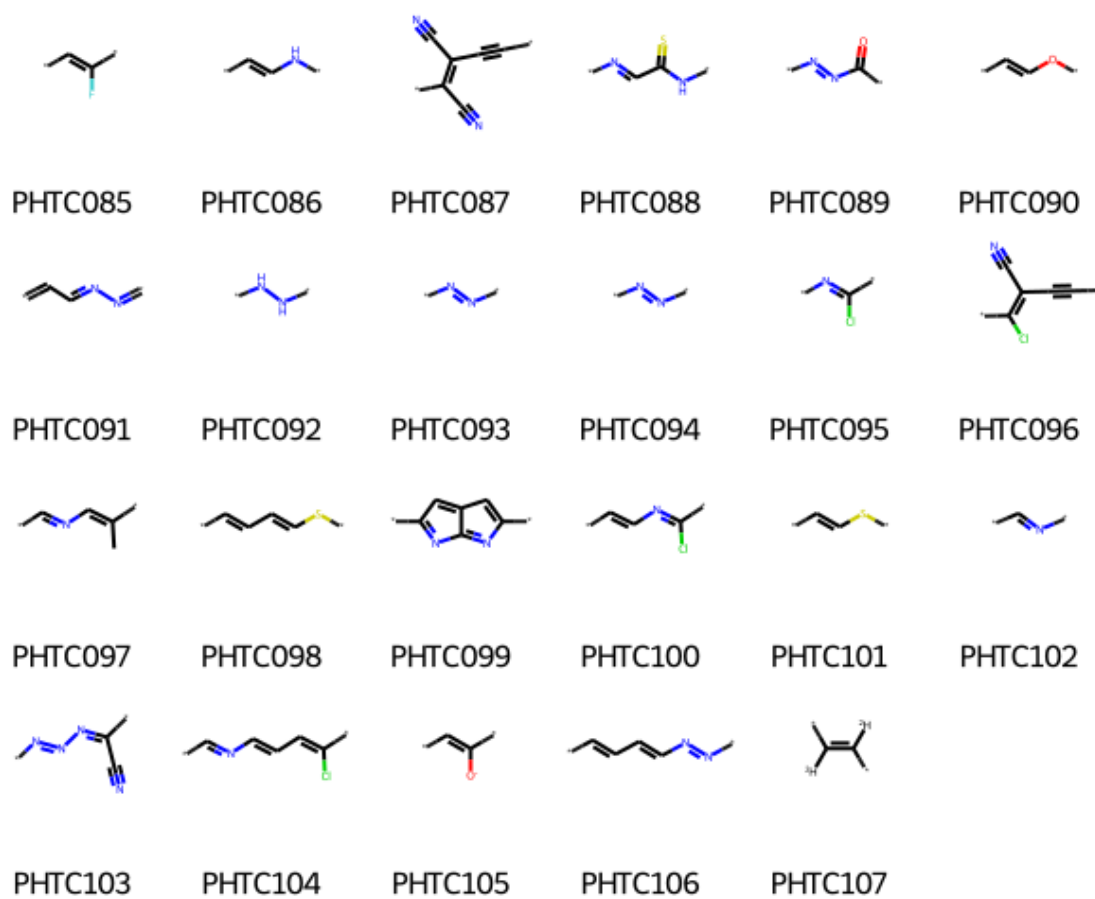


Fig. S8. Polymer monomer structures with TC greater than 20 W/mK verified by MD simulations.

Polymer properties can be found in Table S4 using the PID.

Section S9. Symbolic regression for characterizing the TC of promising polymers

The 107 promising polymer structures ($TC > 20$ W/mK) with optimized descriptors were utilized for symbolic regression (SR), where 20% structures were randomly selected for testing set. The mathematical formulae were acquired and selected using an efficient stepwise strategy with SR based on a genetic programming (GPSR) as implemented in the gplearn code ⁷. At first, Pearson coefficients were used as evaluation metrics of training fitness to filter optimized descriptors and generate sub-descriptors, and the grid search strategy with the hyperparameters listed in Table S5 was applied in GPSR. The hyperparametric combinations corresponding to the 22380 formulas are characterized by complexity and training fitness of Pearson coefficients (PC) as shown in Fig. S9a. The complexity is equivalent to the formula length in gplearn. Among these formulas, 4365 of them with PC values not less than 0.85 are statistically by complexity in Fig. S9b. Generally, the formulas with large complexity have a higher training fitness. But the formulas are also usually quite long and do not facilitate the calculation and analysis. Only formulas with large fitness and low complexity are appropriate, so we selected 158 formulas with the PC value not less than 0.85 and complexity within 10 for subsequent analysis. By counting the frequency of occurrence of the 20 optimized descriptors in 158 formulas, the first 8 descriptors were finally retained, as presented in Fig. S9c. It is worth emphasizing that the MD-inspired descriptors of cross-sectional area (cross-sectional) and dihedral force constants (Kd_average) appeared in each of the formulas. And, we additionally estimated the frequency of occurrence of sub-descriptors created by taking the inverse ($-x$), logarithm ($\ln x$), and so on, as shown in Fig. S9d. As a result, a new ensemble containing 22 descriptors which have a strong association with TC is listed in Table S6 for retraining in gplearn.

Further, we reset the grid search hyperparameters listed in Table S7, and utilized the accuracy R^2 as the evaluation metric. The 19580 formulas with fitting accuracy greater than 0.6 versus complexity are visualized in Fig. S10a. The effective accuracy is the average of the training and testing accuracy. Despite the fact that the effective accuracy of some formulas exceeds 0.8, and their complexity is greater than 50. The Pareto front of accuracy R^2 vs. complexity (no more than 30) of 9073 mathematical formulas shown via density plot in Fig. S10b, and the points of c, d, e and f were identified by Latin hypercube sampling approach ^{8,9}. The formulas for the four points are listed in Table S8, and their fitting results compared with MD labeled $\log_2 TC$ are displayed in Fig. 10c-f. The definitions of the variables x_0 to x_{21} can be found in Table S6.

Table S5. Setup of hyperparameters in gplearn for filter and generate new sub-descriptors

Parameter	Value	Combination
Generations	300	1
Population size in every generation	1000,2000	2
Probability of crossover (pc)	[0.30,0.90], step=0.05	
Subtree mutation (ps)	[(1-pc)/3,(1-pc)/2] (step= 0.01)	746
Hoist mutation (ph)	[(1-pc)/3,(1-pc)/2] (step = 0.01)	
Point mutation (pp)	1-pc-ps-ph	
Function set	{+, -, ×, ÷, \sqrt{x} , $\ln x$, $ x $, $-x$, $1/x$ }	1
Parsimony coefficient	auto	1
Metric	Pearson coefficient	1
Stopping criterial	0.900	1
Random_state	0, 1, 2, 3, 4	5
Init_depth	[2, 6], [4, 8], [6, 10]	3

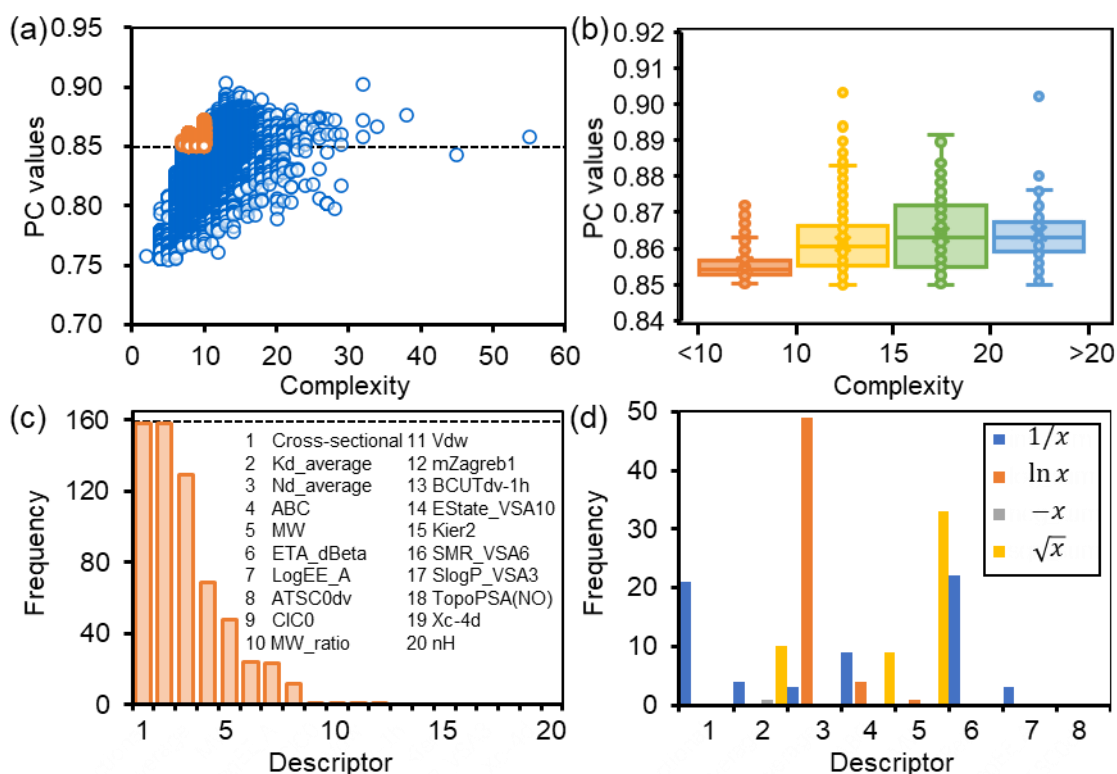


Fig. S9. Filtering optimized descriptors and creating sub-descriptors in gplearn through Pearson coefficient (PC) values. (a) Mathematical formula complexity versus PC values. (b) Statistics of formulas with Pearson coefficient not less than 0.85 by complexity. (c) and (d) Frequency of occurrence of optimized descriptors and sub-descriptors in 158 mathematical formulas (PC values ≥ 0.85 and complexity ≤ 10).

Table S6. New descriptors ensemble for GPSR

Variable	Format	PC values	Variable	Format	PC values
x_0	ABC	-0.37	x_{11}	-ETA_dBeta	0.11
x_1	10/ABC	0.44	x_{12}	Kd_average	0.20
x_2	\sqrt{ABC}	-0.39	x_{13}	$\sqrt{Kd_average}$	0.12
x_3	ATSC0dv	-0.32	x_{14}	LogEE_A	-0.40
x_4	Cross-sectional	-0.52	x_{15}	MW	-0.39
x_5	10/Cross-sectional	0.63	x_{16}	MW/100	-0.39
x_6	1-10/Cross-sectional	0.59	x_{17}	100/MW	0.52
x_7	100/Cross-sectional	0.63	x_{18}	\sqrt{MW}	-0.43
x_8	$\sqrt{100/Cross - sectional}$	0.62	x_{19}	Nd_average	-0.31
x_9	-10/Cross-sectional	-0.63	x_{20}	log Nd_average	-0.35
x_{10}	ETA_dBeta	-0.11	x_{21}	$-\log Nd_average$	0.44

Table S7. Reset of hyperparameters in gplearn for GPSR

Parameter	Value	Combination
Generations	300	1
Population size in every generation	5000	1
Probability of crossover (pc)	[0.30,0.90], step=0.05	
Subtree mutation (ps)	[(1-pc)/3,(1-pc)/2] (step= 0.01)	746
Hoist mutation (ph)	[(1-pc)/3,(1-pc)/2] (step = 0.01)	
Point mutation (pp)	1-pc-ps-ph	
Function set	{+, -, ×, ÷, \sqrt{x} , $\ln x$, $ x $, $-x$, $1/x$ }	1
Parsimony coefficient	0.001, 0.003, 0.005	3
Metric	R^2	1
Stopping criterial	0.900	1
Random_state	0, 1, 2, 3, 4	5
Init_depth	[2, 6], [4, 8], [6, 10], [2, 10]	4

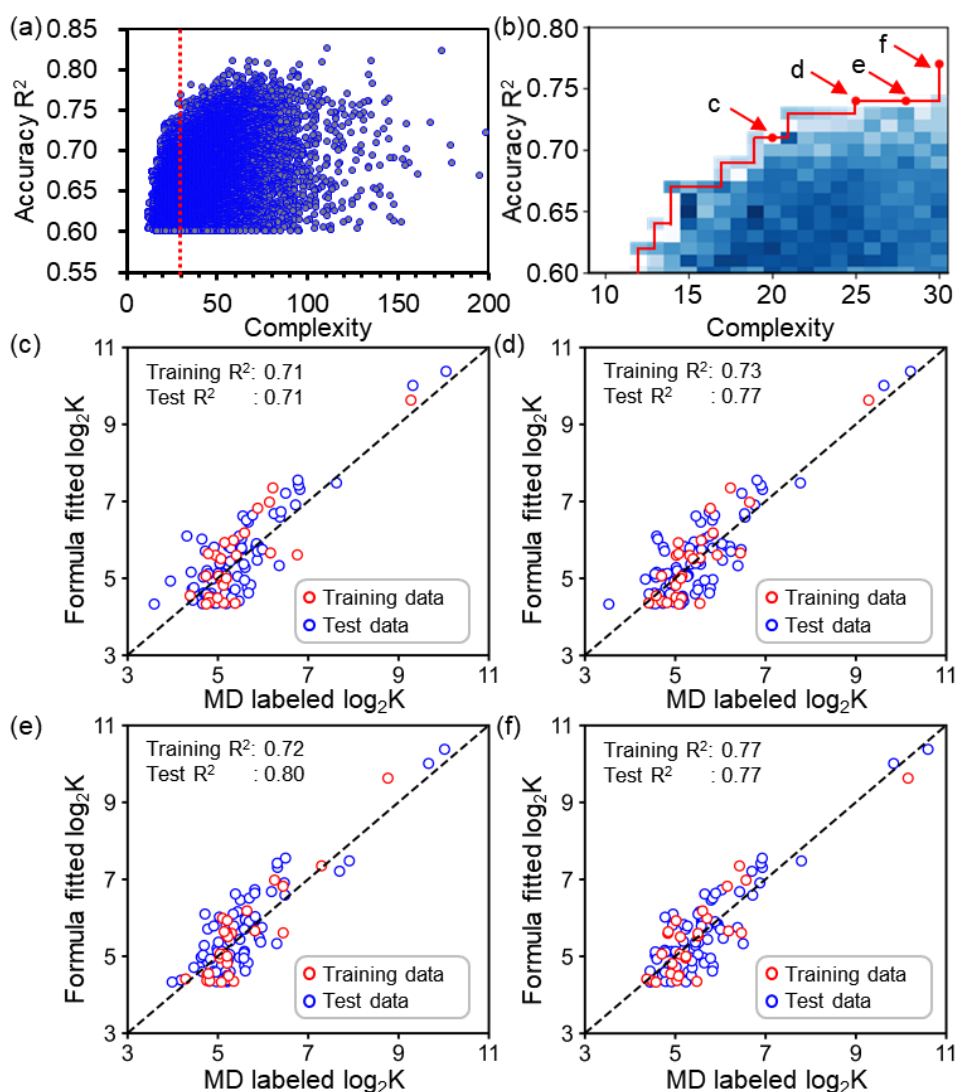


Fig. S10. GPSR for TC prediction of promising polymers. (a) 19580 formulas with fitting accuracy greater than 0.6 versus complexity. (b) Pareto front of accuracy R^2 vs. complexity of 9073 mathematical formulas shown via density plot. The four points of c, d, e and f represent the four formulas at the Pareto front, whose fitting results vs. MD labeled TC are plotted in (c), (d), (e) and (f) respectively.

Table S8. The four mathematical formulas at the Pareto front in Fig. S10b

Point	Formulas	R ²	Complexity
c	$\log_2 K = \sqrt{(x_{12} - x_8 - x_{16} + 0.49) \times x_9 \times (x_6 + x_{20})} + \sqrt{\ln(x_{12})}$ $+ x_{21}$	0.71	20
d	$\log_2 K = \sqrt{x_{12} - \ln \left[(x_8 - x_{11}) \times \frac{x_8}{\ln(\sqrt{x_{19}})} \right] \times (x_6 + x_{20}) \times x_7}$ $+ x_{21} + \sqrt{\ln x_{12}}$	0.74	25
e	$\log_2 K = \ln \left[\frac{1}{x_{10} \times (x_1 - x_2)} - x_{12} \right] \times (x_5 - 0.824)$ $+ \frac{x_{17}}{\sqrt{\frac{x_3}{(x_{12} - x_{11}) \times x_5}}} + x_{21} + x_{13}$	0.74	28
f	$\log_2 K = \sqrt{x_8 + \left[\frac{x_{10}}{\ln(\ln x_{17} - x_{12}) + x_8} - x_{12} \right] \times (x_6 + x_{20}) \times \frac{x_8}{x_{20}}}$ $+ x_{21} + \sqrt{x_{19} - x_{16}}$	0.77	30

References

- 1 Moriwaki, H., Tian, Y.-S., Kawashita, N. & Takagi, T. Mordred: a molecular descriptor calculator. *Journal of Cheminformatics* **10**, 4, doi:10.1186/s13321-018-0258-y (2018).
- 2 Abdi, H. & Williams, L. J. Principal component analysis. *Wiley interdisciplinary reviews: computational statistics* **2**, 433-459 (2010).
- 3 Jaeger, S., Fulle, S. & Turk, S. Mol2vec: Unsupervised Machine Learning Approach with Chemical Intuition. *Journal of Chemical Information and Modeling* **58**, 27-35, doi:10.1021/acs.jcim.7b00616 (2018).
- 4 Durant, J. L., Leland, B. A., Henry, D. R. & Nourse, J. G. Reoptimization of MDL Keys for Use in Drug Discovery. *Journal of Chemical Information and Computer Sciences* **42**, 1273-1280, doi:10.1021/ci010132r (2002).
- 5 Morgan, H. L. The generation of a unique machine description for chemical structures—a technique developed at chemical abstracts service. *Journal of chemical documentation* **5**, 107-113 (1965).
- 6 Lundberg, S. M. & Lee, S.-I. A unified approach to interpreting model predictions. *Advances in neural information processing systems* **30** (2017).
- 7 Stephens, T. *Genetic Programming in Python, with a scikit-learn inspired API: gplearn*, (2022).
- 8 Paulson, N. H., Libera, J. A. & Stan, M. Flame spray pyrolysis optimization via statistics and machine learning. *Materials & Design* **196**, 108972, doi:<https://doi.org/10.1016/j.matdes.2020.108972> (2020).
- 9 Agarwal, G., Doan, H. A., Robertson, L. A., Zhang, L. & Assary, R. S. Discovery of Energy Storage Molecular Materials Using Quantum Chemistry-Guided Multiobjective Bayesian Optimization. *Chemistry of Materials* **33**, 8133-8144, doi:10.1021/acs.chemmater.1c02040 (2021).